Mesoscale Eddies in the Labrador Sea and Their Contribution to Convection and Restratification

Jérôme Chanut, Bernard Barnier, William Large, Laurent Debreu, Thierry Penduff, Jean-Marc Molines, Pierre Mathiot

Mesoscale Eddies in the Labrador Sea and Their Contribution to Convection and Restratification

JÉRÔME CHANUT* AND BERNARD BARNIER

Laboratoire des Ecoulements Géophysiques et Industriels, Grenoble, France

WILLIAM LARGE

National Center for Atmospheric Research, Boulder, Colorado

LAURENT DEBREU

Laboratoire de Modélisation et de Calcul, Grenoble, France

THIERRY PENDUFF, JEAN MARC MOLINES, AND PIERRE MATHIOT

Laboratoire des Ecoulements Géophysiques et Industriels, Grenoble, France

ABSTRACT

The cycle of open ocean deep convection in the Labrador Sea is studied in a realistic, high-resolution (4 km) regional model, embedded in a coarser (⅓°) North Atlantic setup. This configuration allows the simultaneous generation and evolution of three different eddy types that are distinguished by their source region, generation mechanism, and dynamics. Very energetic Irminger Rings (IRs) are generated by barotropic instability of the West Greenland and Irminger Currents (WGC/IC) off Cape Desolation and are characterized by a warm, salty subsurface core. They densely populate the basin north of 58°N, where their eddy kinetic energy (EKE) matches the signal observed by satellite altimetry. Significant levels of EKE are also found offshore of the West Greenland and Labrador coasts, where boundary current eddies (BCEs) are spawned by weakly energetic instabilities all along the boundary current system (BCS). Baroclinic instability of the steep isopycnal slopes that result from a deep convective overturning event produces convective eddies (CEs) of 20–30 km in diameter, as observed and produced in more idealized models, with a distinct seasonal cycle of EKE peaking in April. Sensitivity experiments show that each of these eddy types plays a distinct role in the heat budget of the central Labrador Sea, hence in the convection cycle.

As observed in nature, deep convective mixing is limited to areas where adequate preconditioning can occur, that is, to a small region in the southwestern quadrant of the central basin. To the east, west, and south, BCEs flux heat from the BCS at a rate sufficient to counteract air–sea buoyancy loss. To the north, this eddy flux alone is not enough, but when combined with the effects of Irminger Rings, preconditioning is effectively inhibited here too. Following a deep convective mixing event, the homogeneous convection patch reaches as deep as 2000 m and a horizontal scale on the order of 200 km, as has been observed. Both CEs and BCEs are found to play critical roles in the lateral mixing phase, when the patch restratifies and transforms into Labrador Sea Water (LSW). BCEs extract the necessary heat from the BCS and transport it to the deep convection site, where it fluxed into convective patches by CEs during the initial phase. Later in the phase, BCE heat flux maintains and strengthens the restratification throughout the column, while solar heating establishes a near-surface seasonal stratification. In contrast, IRs appear to rarely enter the deep convection region. However, by virtue of their control on the surface area preconditioned for deep convection and the interannual variability of the associated barotropic instability, they could have an important role in the variability of LSW.

* Current affiliation: MERCATOR OCEAN, Ramonville Saint Agne, France.

Corresponding author address: Dr. Jérôme Chanut, MERCATOR OCEAN, 8/10 rue Hermès, Parc Technologique du Canal, 31520 Ramonville Saint Agne, France.
E-mail: jchanut@mercator-ocean.fr

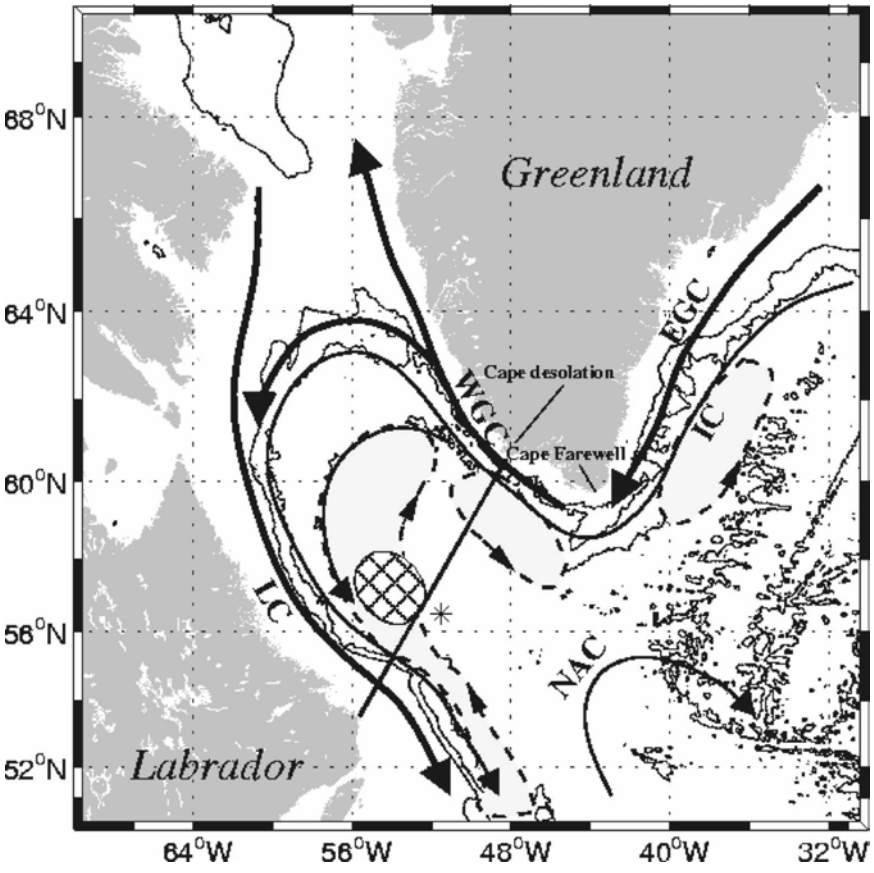

FIG. 1. Sketch of the circulation in the Labrador Sea. EGC and WGC are the East and West Greenland Currents, respectively. LC is the Labrador Current, IC is the Irminger Current, and NAC is the North Atlantic Current. Dashed lines correspond to the middepth cyclonic recirculations reported by Lavender et al. (2000). Also displayed on this sketch are the WOCE AR7W hydrographic line (thick black line) and the OWS Bravo (star). Isobaths 1000, 2000, and 3000 m and the location of the deep convection site (shaded ellipse) after Pickart et al. (2002) are shown.

1. Introduction

The Labrador Sea is one of the few sites where a reoccurring cycle of open ocean deep convection is known to occur (Marshall and Schott 1999). The preconditioning phase of this cycle sets the stage for deep convective mixing or overturning, which is then followed by a phase of lateral exchange and spreading. This third phase is characterized by a restratification of the entire water column. Critical to preconditioning, the Labrador Sea is its cyclonic subpolar gyre circulation (Fig. 1), where the doming of isopycnals brings weakly stratified interior water closer to the surface. The other major element is a strong surface buoyancy loss throughout fall and winter, which erodes the seasonal stratification formed during summer heating. Thus, midwinter ocean conditions favor deep convective overturning events that are triggered intermittently by vigorous buoyancy loss when strong, cold winds blow off the Labrador coast. The associated surface heat and buoyancy fluxes can exceed 1000 W m^{-2} and 10^{-7} m^2 s^{-3}, respectively. The net result is a homogeneous patch extending as deep as 2000 m, and 200 km laterally. This patch is surrounded by horizontal density gradients that are baroclinically unstable. Its disintegration mixes laterally until the patch is restratified and the entire region attains the relatively uniform water mass characteristics of Labrador Sea Water (LSW; Clarke and Gascard 1983). Of particular climatic importance is the subsequent advective spreading of LSW as an intermediate water mass throughout the North Atlantic Ocean.

The deep convection cycle in the Labrador Sea exhibits considerable interannual variability, which is correlated with the strength of the wintertime surface heat loss and, more generally, with the dominant mode of regional atmospheric variability: the North Atlantic Os-

cillation (Pickart et al. 2002). However, the concept of a year-to-year direct response to atmospheric forcing remains too simplistic to understand and predict the deep convection cycle. A highly uncertain factor is the ocean's behavior during the third phase, when the buoyancy stratification is at least partially restored. At the former Ocean Weather Station (OWS) Bravo (Fig. 1), observations show a relatively rapid warming of intermediate layers after the conclusion of the convective overturning phase, which cannot be explained by the relatively weak spring and summer solar heating (Lilly et al. 1999), but rather a lateral advective process is suggested. This warming might be incomplete in the case of repeated cold winters, which strengthen the deep convective overturning by progressively eroding the stratification (Lazier et al. 2002). Thus, restratification need not be complete, allowing the basin to remember previous winters. This memory leads to a close coupling between the response of the ocean's lateral processes and the vertical mixing forced by the atmosphere. In a coupled ice–ocean model, Mizoguchi et al. (2003) further demonstrate the importance of the interior's autumnal stratification in modeling interdecadal variability of the deep convection cycle.

The cyclonic upper Labrador Sea circulation (Fig. 1) is composed of three currents. On the Greenland shelf, the West Greenland Current (WGC) flows northward. Farther offshore, tracking the 1000-m isobath, the subsurface Irminger Current (IC) carries warm and salty water of subtropical origin (Cuny et al. 2002) to the north. Along the western shelf, the Labrador Current (LC) transports cold and freshwaters of Arctic Ocean origin. Other currents of interest are the northwest corner of the North Atlantic Current (NAC), which bounds the basin to the south, and the abyssal deep western boundary current, which circulates dense water from the Denmark Strait Overflow southward to the western North Atlantic. The central basin has a weak mean circulation but intense eddy activity, which has been recently observed (Prater 2002; Lilly et al. 2003). Lateral heat exchange, across the Labrador Basin, could therefore be accomplished through mesoscale eddy processes. This hypothesis is supported by numerical experiments that have considered eddies generated by a number of mechanisms.

First, the baroclinic instability of the convective patch itself generates convective eddies (CEs). Numerical studies of open ocean deep convection (e.g., Visbeck et al. 1996; Jones and Marshall 1997) have demonstrated the ability of CEs to reduce the depth of convective overturning and ultimately to disperse the convective patch during the lateral exchange phase. Indeed, Lilly et al. (2003) observed the signature of similar eddies with a diameter of about 20–30 km. The numerical results are the basis of most of the scaling developed for the dynamics of deep convective mixing (Marshall and Schott 1999), but the rather idealized model setups are an experimental weakness. In addition, the instability of the boundary current system (BCS) could be an important source of what will be referred to as boundary current eddies (BCEs). This process has been studied by Spall (2004), who describes the equilibration of a semienclosed marginal sea as a balance between mean advection by the BCS, surface fluxes and lateral transport by BCEs. Also, offshore of Cape Desolation (Fig. 1) appears to be a localized source of eddies known as Irminger Rings (IRs). Analysis of satellite altimeter and mooring data (Lilly et al. 2003) shows a pronounced maximum in eddy kinetic energy (EKE) associated with the periodic shedding of warm, salty IRs of 40–50 km in diameter and predominantly anticyclonic. This process has been successfully simulated in a $\frac{1}{12}^\circ$ North Atlantic model by Eden and Böning (2002), who show that the instability is mainly barotropic and triggered by the horizontal shear induced by the sudden change of the topographic slope near Cape Desolation. They link the seasonality, maximum generation in winter, to the modulation of the WGC–IC system driven by wind stress variations, but they do not consider the propagation of Irminger Rings toward the central basin, where satellite altimeters measure an EKE maximum in late winter. In a highly simplified model of the Labrador Sea, Katsman et al. (2004) reproduce the BCS and localized IR generation and conclude that these eddies may be more efficient than CEs in restratifying the convective patch. According to their analysis, IRs transfer 55% to 98% of the lateral heat flux required to balance the annual surface heat loss. Finally, the NAC appears to generate noticeable mesoscale eddy activity at the southern margins of the Labrador Sea.

The present study focuses on the influence of mesoscale eddies in the Labrador Sea. Realistic modeling allows the interplay of different eddy types, as distinguished above, over a number of years. The first objective is to characterize the roles of each type in the region where deep convective mixing is observed to occur in the Labrador Sea. Specific questions are the roles of eddies in setting the location of deep convective mixing and in restratifying the convective patch, from the CE time scale to the seasonal cycle. A particular focus is on the lateral, middepth (seasonal thermocline to the bottom of the convective patch) heat transfer that is responsible for the reconstruction of the temperature

profile. The second objective is to quantify the role of mesoscale eddies in the heat budget of the central Labrador Sea and, in particular, in balancing the surface heat flux. It is motivated by the importance of heat flux to seasonal stratification, preconditioning, triggering convective events and restratification. A key modeling challenge is for the eddies to flux sufficient heat to achieve a realistic equilibrium over the time scale of several years. Neither the near- surface stratification nor the flux of salt and freshwater is addressed.

These questions relate to the variability of open ocean deep convection. If BCEs and CEs dominate the lateral flux to the interior, then it can be argued (Jones and Marshall 1997; Spall 2004; Straneo 2006) that the eddy fluxes should scale as the square of the lateral temperature/buoyancy gradient. But if IRs are important, then so are the large-scale circulation and its forcing. The study is directly relevant to the parameterization of mesoscale eddy effects in coarse and eddy-permitting resolution ocean models. Existing schemes, such as Gent and McWilliams (1990), are constructed to mimic local baroclinic instability, but not CEs where the isopycnic slopes are too steep nor the generation and remote transport of IRs.

The paper is organized as follows: section 2 describes the embedded model configuration and the various sensitivity experiments. It is followed in section 3 by an examination of the time-dependent and mean circulation produced by a 10-yr integration of the model. Properties of the boundary current, the eddy flow, and the seasonal cycle of convection are analyzed, and the realism of their representation is evaluated. Section 4 investigates the generation of mesoscale eddies in the Labrador Sea. Using sensitivity experiments with a different (smoothing of the) topography, the analysis identifies and separates the major sources of eddies. Section 5 describes the role of eddies in the heat budget of the basin's interior. Conclusions are presented in section 6.

2. Model configuration

Due to the low radius of deformation in the Labrador Sea (≈7 km), a high horizontal resolution is needed to accurately model eddy processes, which in turn leads to high computation costs. As a matter of fact, few high-resolution, realistic regional studies of the Labrador Sea have been documented so far. Eden and Böning (2002) have shown in the 1/12° North Atlantic model developed in the context of the Family of Linked Atlantic Model Experiments (FLAME) that a realistic level of eddy kinetic energy can be simulated. Another attempt is a regional 1/10° model of the Labrador Sea with open boundaries designed for the LabSea experiment (Marshall et al. 1998; Marshall and Schott 1999).

As an alternative to these configurations, a grid refinement technique is used in the following. This type of method has shown its robustness in idealized and realistic oceanographic applications [barotropic modon in Spall and Holland (1991); the baroclinic vortex propagation in Fox and Maskell (1995); the central California upwelling in Penven et al. (2006); the Iceland-Faeroe front in Fox and Maskell (1996)]. It has the advantage to allow a very high local horizontal resolution without suffering from the high computation costs of a basin scale model or specifying lateral boundary conditions for the area of interest.

Our embedded system, detailed in the next subsections, consists of a state-of-the-art ~1/3° resolution, primitive equation realistic model of the North Atlantic with a ~1/15° in the Labrador Sea.

a. Numerical model

The numerical model used in this study is the ocean general circulation model Océan Parallélisé (OPA) 8.1, developed by Madec et al. (1998). It solves the three-dimensional primitive equations in spherical coordinates discretized on a C grid and fixed vertical levels (z coordinate), assuming hydrostatic equilibrium, the Boussinesq and rigid-lid approximations. Surface boundary layer mixing is parameterized according to the 1.5 turbulent closure model of Gaspar et al. (1990), adapted to OPA by Blanke and Delecluse (1993). In case of static instability, a viscosity/diffusivity enhancement of 1 $m^2 s^{-1}$ is used. A horizontal biharmonic operator is used for the parameterization of the lateral subgrid-scale mixing for both tracers and momentum. The coefficient (defined as A_b at the equator in Table 1) is proportional to the third power of the cosine of the local latitude. Side-wall boundary conditions are free slip. Density is computed after the nonlinear equation of state of Jackett and McDougall (1995).

b. Embedded system

1) Coarse-grid North Atlantic model—NATL3

The large-scale, eddy-permitting-resolution North Atlantic model (NATL3) is very similar to the one defined in the DYNAMO project (Willebrand et al. 2001). It uses a Mercator isotropic longitude × latitude grid of resolution 1/3° × 1/3° cosϕ (ϕ being latitude), spanning the North Atlantic from 20°S to 70°N (Fig. 2). The horizontal resolution in the Labrador Sea is about 20 km. The vertical resolution comprises 43 levels

TABLE 1. Model experiments and parameters.

Name of expt	Horizontal resolution	No. of horizontal grid points	Time step (min)	Biharmonic viscosity A_b ($m^4 s^{-1}$)	Bathymetry (Smith and Sandwell 1997)
Fine-grid model (LAB15)					
SMBAT	1/15°	432 × 322	8	-2.0×10^9	on 1/3°
REBAT	1/15°	432 × 322	8	-2.0×10^9	on 1/15°
Coarse-grid model (NATL3)					
NATL3	1/3°	358 × 361	40	-2.5×10^{11}	on 1/3°

spaced from 12 m at the surface to 200 m below 1500 m. The bathymetry is calculated by bilinear interpolation of the Smith and Sandwell (1997) dataset. Northern and southern boundaries are closed, and the model is restored to the climatology of Reynaud et al. (1998) in buffer zones located in the Nordic Seas at the southern boundary and in the Mediterranean Sea.

The forcing, a climatological annual cycle of wind

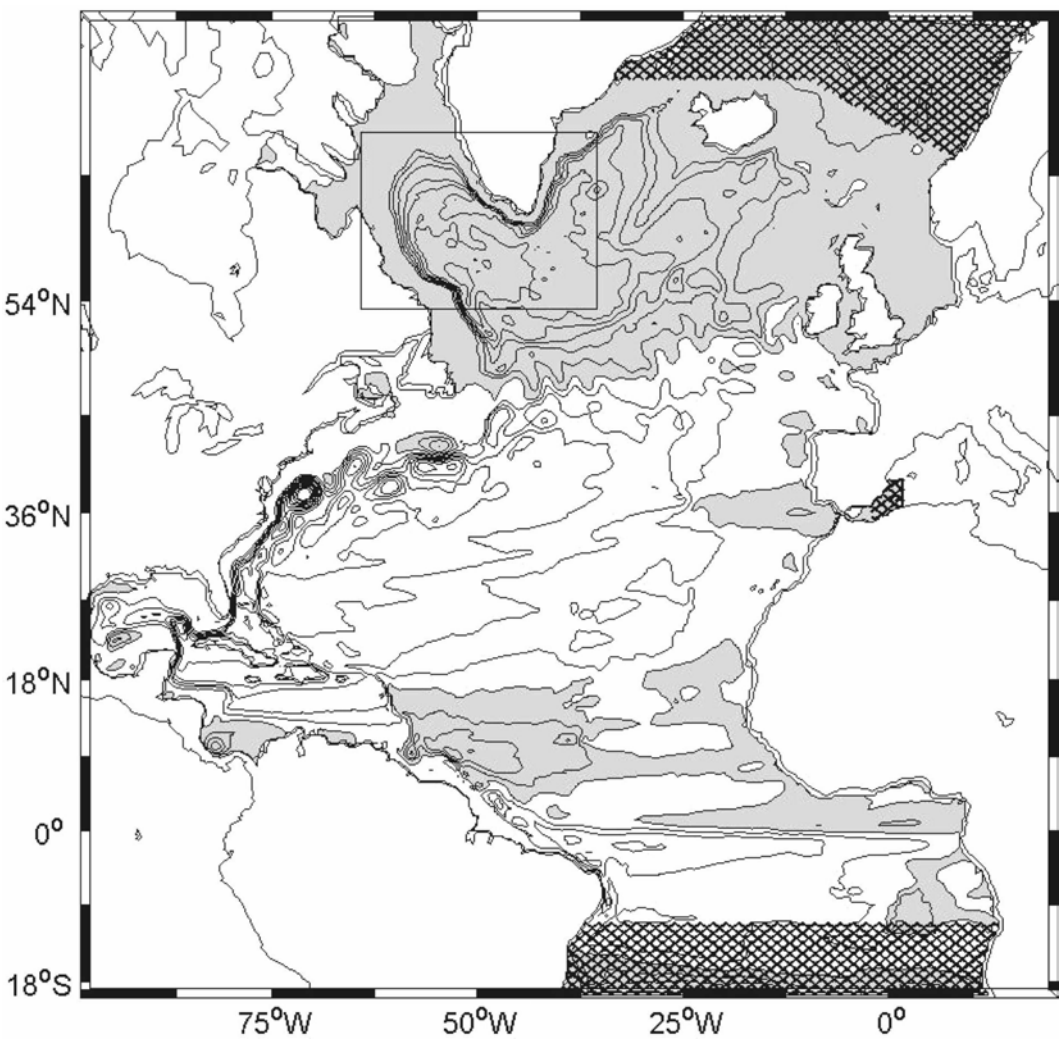

FIG. 2. North Atlantic 1/3° model NATL3. Model domain and 5-yr mean barotropic streamfunction (REBAT experiment). Negative areas are shaded, and contour interval (CI) is 5 Sv. Relaxation areas in the Nordic Seas, at the Southern Boundary, and in the Mediterranean Sea are hatched. The frame indicates the position of the embedded 1/15° grid.

stress, heat, and freshwater fluxes, is based on the monthly mean fields obtained by averaging the European Centre for Medium-Range Weather Forecasts (ECMWF) reanalysis between 1979 and 1993 (Garnier et al. 2000). Surface heat flux is formulated based on Barnier et al. (1995). The sea surface temperature (SST) field of Reynolds and Smith (1994) and spatially and seasonally varying restoring parameter from ECMWF analyses are used in the calculation of the flux correction (the relaxation time scale for the top layer is about 12 days). The evaporation minus precipitation ($E - P$) flux is expressed as a virtual salt flux (Barnier 1998), including river runoff. Surface salinity (SSS) is, in addition, relaxed to the surface salinity climatology of Reynaud et al. (1998) with a time scale identical to that given by the formulation of the heat flux correction. Because no independent prognostic sea ice model is used, sea ice coverage is deduced both from a monthly climatological dataset and whenever the model SST falls below the freezing point. In this case, surface fluxes are set to zero and surface values of SST and SSS are respectively relaxed to freezing temperature and climatological salinity (with a 3-day time scale).

2) Fine-grid Labrador Sea model—LAB15

The fine-grid Labrador Sea model (LAB15) is a local refinement of NATL3 in the region of the Labrador and most of the Irminger Basins (53.4° to 64.4°N, 64.2° to 35.4°W; Fig. 2). The refinement factor is 5, which gives a horizontal resolution of $\frac{1}{15}° \times \frac{1}{15}° \cos(\phi)$ ($\approx$4 km). It is embedded into NATL3 via the Adaptive Grid Refinement in FORTRAN (AGRIF) package (Blayo and Debreu 1999; Debreu et al. 2005). The main characteristic of the present implementation of AGRIF used here allows an interactive (i.e., two way) integration of the two grids and is described in the appendix. The forcing of LAB15 is a bilinear interpolation of the NATL3 forcing.

The bottom topography of the LAB15 model is calculated on the $\frac{1}{15}°$ grid by bilinear interpolation of the original Smith and Sandwell (1997) dataset. It retains all the details that can be resolved at that resolution. This fine realistic bathymetry (REBAT) is used in most model simulations of the embedded model system.

As demonstrated by Katsman et al. (2004) in idealized channel experiments and Eden and Böning (2002) in a primitive equation, realistic model setup, the topographic details near Cape Desolation control the boundary current meandering and the subsequent shedding of Irminger Rings. This inspired us to smooth the bathymetry for LAB15 to artificially suppress the Irminger Rings' generation and enlighten other sources of eddy variability that could be masked by the propagation of these rings in the interior. Therefore, a smoothed bathymetry (SMBAT) was constructed. It is a bilinear interpolation of the bottom topography of the $\frac{1}{3}°$ NATL3 configuration and does not represent details finer than this $\frac{1}{3}°$ scale. As demonstrated in section 4, this smoothing yields a more stable boundary current.

3) Model experiments

Every experiment has been initialized at rest with the mid-September fields of temperature and salinity interpolated from the seasonal climatology of Reynaud et al. (1998). This summertime period roughly corresponds to the maximum stratification in the basin interior. All are run for 10 yr, with the climatological annual forcing applied in a cycling way.

The first experiment has run NATL3 alone. After 10 yr, the solution is very similar to Fig. 2 throughout the coarse-grid domain. Also, it is very consistent with that produced by models at that resolution, as presented in the DYNAMO experiment (Willebrand et al. 2001). In particular, the barotropic transport over the North Atlantic in Fig. 2 shows that a realistic large-scale circulation is achieved in the subpolar gyre, with a 37 Sv (1 Sv $\equiv 10^6$ m^3 s^{-1}) transport in the boundary current.

Two experiments have been carried out with the embedded system (see Table 1), which differ only by the bottom topography used in the fine-grid model. The REBAT experiment uses the realistic topography, whereas the SMBAT experiment uses the smooth topography.

An example of instantaneous potential temperature in year 6 in REBAT, given in Fig. 3c, shows the contrast in the turbulent scales between the two grids and the good matching at the interface. After 4 yr of integration, a quasi equilibrium in the total kinetic energy is obtained in the refined area (Fig. 4a), with a well-marked seasonal cycle. The basin-averaged (over the LAB15 model area) potential temperature (Fig. 4b) equilibrates within about 6 yr. Salinity still shows a drift after 10 yr (Fig. 4c); a similar drift is also noticed in the NATL3 basin average as in most North Atlantic models (Treguier et al. 2005). This is just a consequence of the difficulty in specifying salinity forcing at the long time scales involved. Local evolution (see section 5) also suggests a quasi equilibration of the system after the same 4- to 5-yr time. In the following diagnostics, mean states are built using the last 5 yr of each experiment with instantaneous fields spaced by 2 days. Model solutions are discussed in the next three sections. In any case, drifts are identical between REBAT and SMBAT

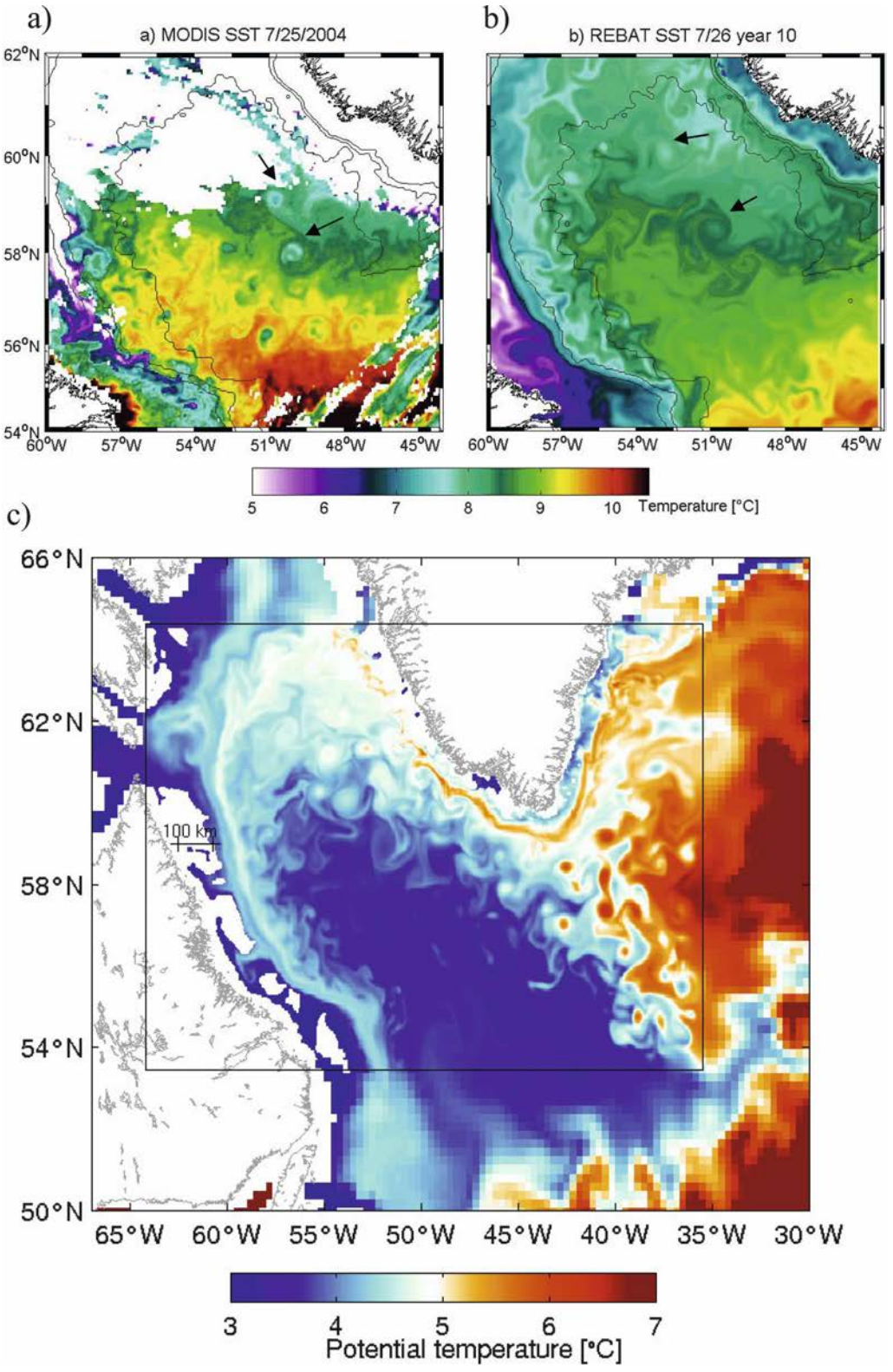

FIG. 3. (a) MODIS SST taken from *Aqua* satellite on 25 Jul 2004. (b) Model SST in July of year 10 (REBAT experiment). Arrows indicate Irminger Rings. (c) Map of instantaneous potential temperature at 182 m in the REBAT experiment in November of year 6. Color contours are not interpolated to enlighten the horizontal-grid resolution difference between the two grids.

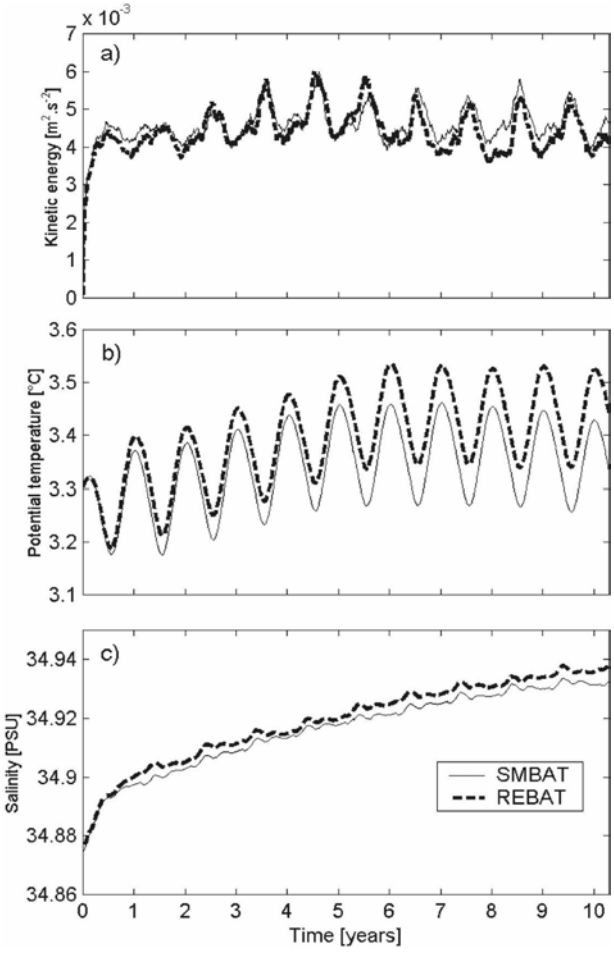

FIG. 4. Time evolution of the basin average (over the refined grid) of (a) total kinetic energy, (b) potential temperature, and (c) salinity. Year 0 starts in mid-September. Thin line: SMBAT experiment; thick dashed line: REBAT experiment.

experiments so they will not hamper what can be learned from their comparison.

3. Circulation characteristics in the REBAT experiment

a. Instantaneous flow

A snapshot of the model sea surface temperature (Fig. 3b) in July of year 10 shows a high density of fine mesoscale structures in the basin interior. These consists of filaments extending from the offshore sides of the cold-surface boundary currents (the WGC and the LC), mushroom-shaped patterns, and few coherent circular eddies. Most of the latter, such as the cold anomaly at 58.5°N, 51°W, are the so-called Irminger Rings. Very similar patterns can be seen on a rare view of the basin given by the Moderate Resolution Imaging

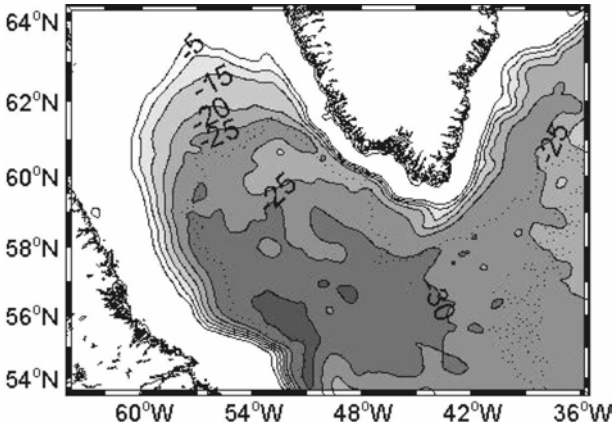

FIG. 5. Barotropic streamfunction (Sv) averaged over the last 5 yr of REBAT experiment. Contour interval is 5 Sv.

Spectroradiometer (MODIS) satellite image taken on the 25 July 2004 (Fig. 3a). Apart from the evident presence of IRs, this high-resolution picture (4 km) confirms the intense mesoscale activity of the basin interior, which is well captured by the model.

The subsurface circulation can be discussed from the snapshot of potential temperature at about 200 m displayed on Fig. 3c (see model animations at http://meolipc.hmg.inpg.fr/Web/TEMP/JPO-Mov/). The Irminger Current (depicted by the thin band of relatively warm temperature along Greenland) enters the LAB15 domain by the northwestern corner as a relatively warm current (≈5.5°C), compared to the interior Labrador Sea (<4°C). As it circulates, the current becomes colder. This cooling is evident at all depths, which suggests that the boundary current gives up part of its heat to the interior waters through turbulent mixing. Mesoscale eddies are numerous on the outer side of the current. As it exits the LAB15 domain at its southern limit (54°N), the boundary current goes through the boundary and smoothly becomes a broad current characteristic of the ⅓° solution. It is then more than 1°C colder than it was when entering the Labrador Sea. At the end of winter, the center of the Labrador Sea appears as a pool of rather cold water (<3.5°C). A similar picture comparing the temperature field in March and September (see Figs. 10a,b) shows that the pool of cold water has significantly shrunk in early fall, suggesting that eddies are bringing warmer water from the boundary current to the interior ocean. This is illustrated in section 5.

b. Mean circulation

The vertically averaged mean circulation is shown in Fig. 5. The maximum transport in the basin is 37 Sv, in

line with the 44-Sv estimate of Pickart et al. (2002). Swift currents encircle the basin inshore the 2000-m isobath, with a maximum surface speed (not shown) of 70 cm s^{-1} near Cape Desolation. It is in general agreement with the circulation pictured by Cuny et al. (2002) from surface drifters. In the northwestern part of the basin, in situ observations (Cuny et al. 2002; Lavender et al. 2000) show that the WGC–IC splits in two distinct branches near Cape Desolation, following the 2000- and 3000-m isobaths. The experiment REBAT, with realistic fine-resolution bathymetry, tends to represent this peculiarity, while in the SMBAT experiments (not shown) the time-averaged flow closely follows the 2000-m isobath around the basin.

A series of weak inner counter currents (i.e., opposite to the main direction of the rim current) in the interior Labrador Sea, forming closed cyclonic recirculations, has been revealed by Lavender et al. (2000; see sketch on Fig. 1). Those are suspected to favor the localization of deep convection in the southwest part of the basin (Pickart et al. 2002). They could also explain the spreading of LSW water in the Irminger Basin (Straneo et al. 2003). No such counter flows, at least on the Greenland side, are visible in any of our experiments (Fig. 5). The crude representation of the steep slopes of the basin boundaries, due to the z-coordinate vertical discretization could explain this behavior. Käse et al. (2001) have indeed shown that these recirculations are greatly enhanced with partial cell representation of the bottom topography (not used here). However, the modeled 10-Sv cyclonic recirculation, on the Labrador side through the fine-grid south boundary, seems realistic (10 to 14 Sv according to Fischer et al. 2004).

c. Surface eddy kinetic energy

The model surface eddy kinetic energy is defined as

$$\text{eke} = \frac{1}{2}(\overline{u'^2} + \overline{v'^2}), \tag{1}$$

where the overbar represents a seasonal time average (January–March, April–June, and so forth) over the last 5 yr of each experiment to account for the seasonal cycle and (u', v') are the deviations of the surface horizontal velocities from this average. The annual mean shown in Fig. 6b for REBAT can be compared with an estimate derived from Ocean Topography Experiment (TOPEX) satellite altimeter measurements between 1994–2000 computed by Lilly et al. (2003; Fig. 6a). The model EKE has a maximum of about 350 $cm^2\ s^{-2}$ on the west coast of Greenland at 61°N, as seen in the observations, related to the local shear instability of the WGC–IC. Its magnitude is somewhat lower than the estimate of Lilly et al. (2003) (500 $cm^2\ s^{-2}$), but the latter figures as an upper bound in the reported range [e.g., different data processing as in Ducet et al. (2000) gives a maximum of 200 $cm^2\ s^{-2}$]. Overall, the pattern of the maximum and its offshore decay appear rather well reproduced by the model.

Besides the WGC instability at 61°N, a weaker maximum is found in the LC, but it is confined in shallow, cold waters (<200 m) along the Labrador coast. Thus, it does not concern the warm intermediate waters of the IC. Finally, note that the mesoscale activity from the northwest corner of the NAC seen around 54°N, 46°W in observations is almost absent in the model. This is a bias of the NATL3 model in which the NAC is indeed too far south (Fig. 2).

d. Mean hydrography

To examine the mean thermohaline properties, we focus on the World Ocean Circulation Experiment (WOCE) AR7W section between Hamilton Bank, Labrador, and Cape Desolation on the west coast of Greenland (Fig. 1). In the '90s, numerous hydrographic surveys (most of the time in late spring) were carried out on this line, so that it probably provides the best known picture of both the boundary currents and the interior hydrographic properties. The reader is referred to Pickart et al. (2002), Cuny et al. (2002), Lazier et al. (2002), or Lilly et al. (2003) for examples of such sections.

As a reference, we will use in the following an annual mean section from the hydrographic dataset of the Bedford Institute of Oceanography (data courtesy of Igor Yashayaev 2006, personal communication). Corresponding potential temperature and potential density contours are shown in Fig. 7a. Near the surface, the West Greenland Current is distinguishable with cool (and fresh) water ($T < 3.5$°C, $S < 34.8$ psu). It flows northward around the basin to become the LC on the Labrador side with similar properties. These low-density currents lie over the warm and salty core of the Irminger Current ($T \approx 4.5$°C, $S \approx 34.9$ psu) that loses part of its heat through mixing along isopycnal surfaces and atmospheric cooling on its way around the basin (Cuny et al. 2002). The basin's interior is filled with convectively formed Labrador Sea Water at middepths (1000–2000 m) and strongly stratified waters below 2000 m, corresponding to North Atlantic Deep Water and Denmark Strait Overflow Water.

In the model counterpart shown in Fig. 7b, boundary currents appear too warm (and too salty), as in most North Atlantic Ocean models (Treguier et al. 2005). One has to keep in mind that the climatological dataset has a relatively low resolution (⅓°), and it certainly

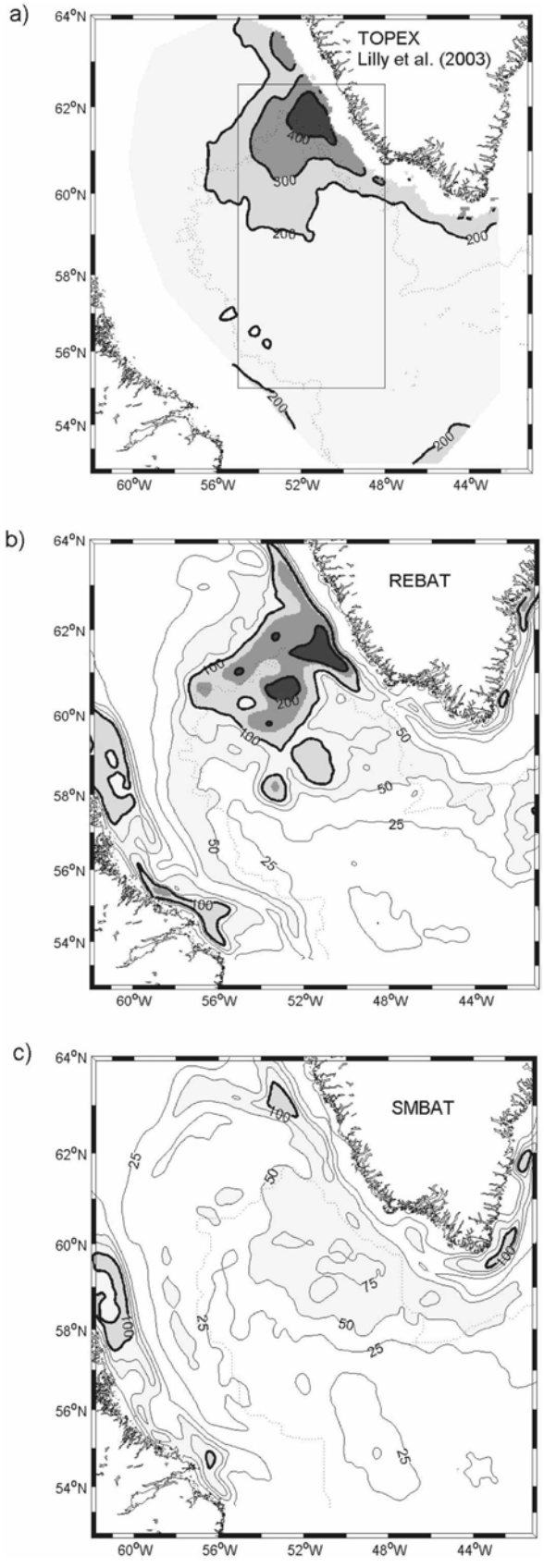

misses the narrow temperature maximum of the IC. One of the most serious issues in the model simulations is perhaps the vertical structure of the BCS near the surface. The LC and WGC are indeed trapped on the shelf break so that the 200 thick, cold (and fresh) water cap over the IC is not well represented. Nevertheless, these temperature–salinity biases partially compensate in the upper 1500 m, so that the vertical structure of density is reasonably well reproduced in the boundary currents.

As it will be shown in section 5, the interior's properties are partly set up by both lateral exchanges with the boundary current and atmospheric forcing. It follows that they should somehow reflect the BCS biases. The interior is indeed 0.2°C warmer and 0.1 psu saltier than in observations (Fig. 7c). Nevertheless, the temperature vertical stratification agrees well with the observed, but the salinity profile is too weakly stratified. This may be a consequence of the lack of freshwater in the surface boundary currents that would have been fluxed by eddies in the interior and transferred at depth through wintertime mixing. The resulting density stratification appears weaker than in the climatology deduced from observations (shown in Fig. 9) between 200 and 2000 m but similar to the observed conditions in the mid-1990s after 5 yr of high-convection winters (Lilly et al. 2003). This does not change much the deformation radius of the first baroclinic mode, hence the expected eddy length scales (6 km instead of 7 km in observations). Finally, note the rising of isotherms shifted to the Labrador side, also visible in observations. It is characteristic of the area where the stratification is preferentially eroded by the wintertime convection.

e. Deep convection

At the end of winter, the center of the Labrador Sea appears as a pool of rather cold (around 3.2°C) and homogeneous water (Fig. 10a). A snapshot of the winter mixed layer depth in late March is shown in Fig. 8a. This figure reveals that maximum mixed layer depths (around 2000 m) are located on the Labrador side of the sea (south of 60°N), in agreement with wintertime

←

FIG. 6. (a) Surface EKE ($cm^2\ s^{-2}$) deduced from TOPEX satellite altimeter between 1994 and 2000 (data courtesy of J. Lilly 2005, personal communication). (b) Surface EKE ($cm^2\ s^{-2}$) for REBAT experiment. (c) Same as (b), but for SMBAT experiment. Thick line contour interval is 100 $cm^2\ s^{-2}$, while thin line contour interval is 25 $cm^2\ s^{-2}$ and for EKE lower than 100 $cm^2\ s^{-2}$ only. For (b) and (c), an 11-point Hanning filter has been applied prior to plotting.

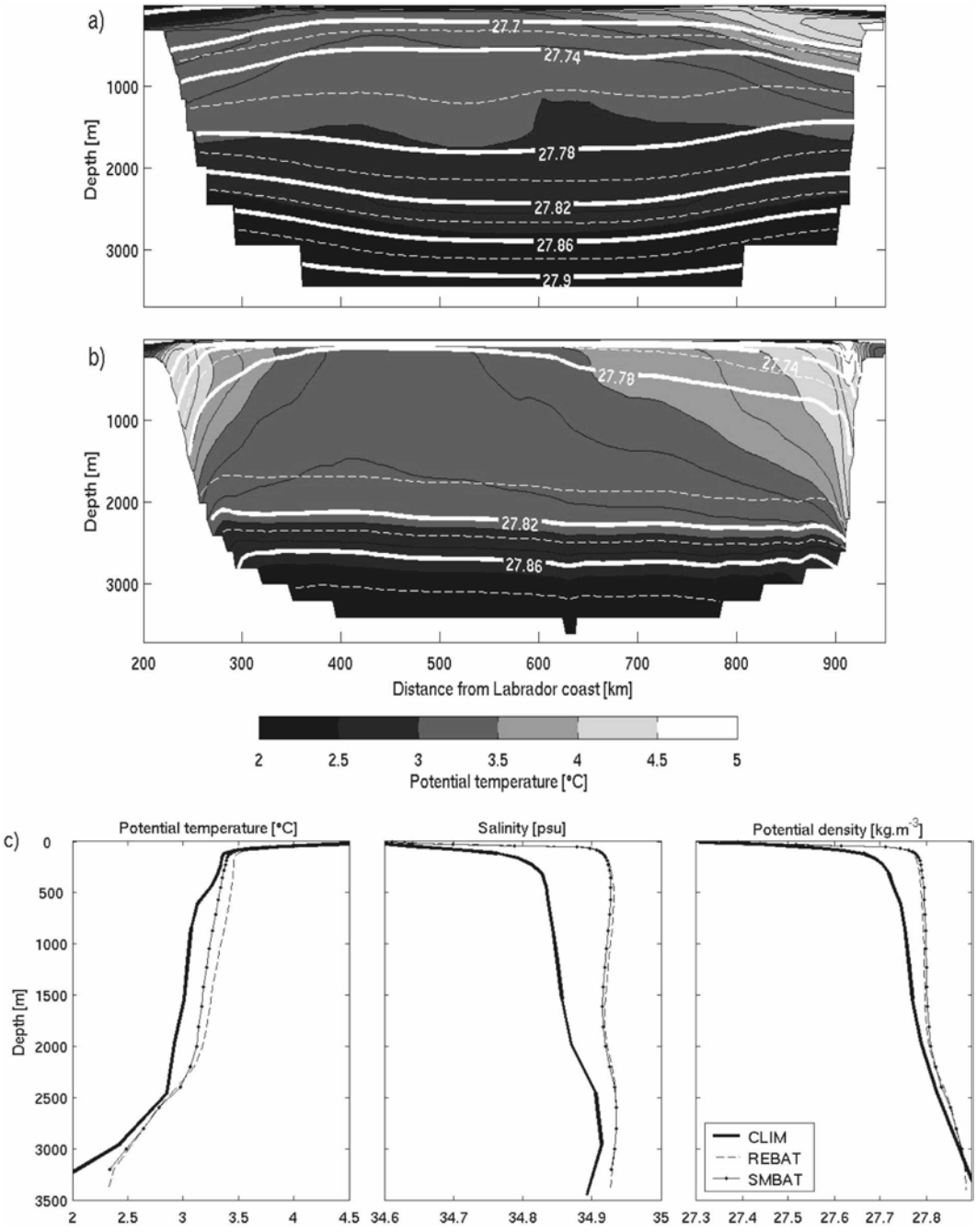

FIG. 7. (a), (b) AR7W sections of potential temperature (see Fig. 1) with potential density contours overlayed. (a) Climatological section (data courtesy of I. Yashayev 2006, personal communication). (b) REBAT experiment. (c) Model and climatological profiles of potential temperature, salinity, and potential density averaged between 400 and 700 km along AR7W section.

surveys of Clarke and Gascard (1983) and Pickart et al. (2002). Model mixed layer depths are deeper than generally observed values but nevertheless observed during periods of intense convection (e.g., in the early 1990s; Lazier et al. 2002). Conditions simulated by the model should be seen as representing a period of intense deep convection. This can be explained by the relatively low mean density stratification in the model simulations (see previous subsection) and also by the repeated high annual heat loss induced by the surface flux correction (see section 5).

A vertical view of deep convection is given by the

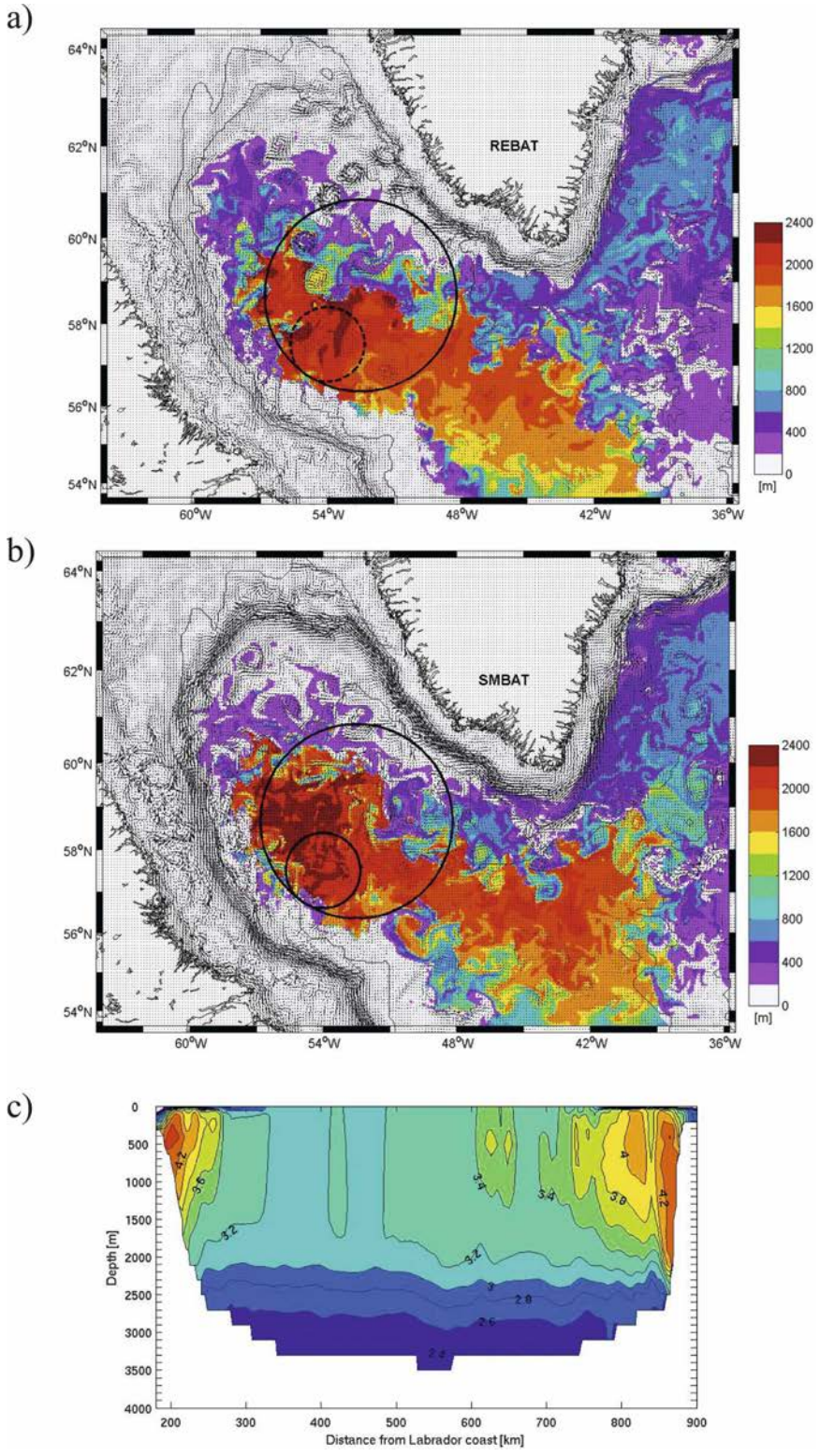

FIG. 8. Snapshots of the mixed layer depth in meters at the end of March in year 8 of the (a) REBAT experiment and (b) SMBAT, defined as the depth where potential density exceeds the surface density by 0.005 kg m^{-3}. Surface velocity vectors are overlaid (one vector every two grid points). The largest circle corresponds to the interior region, while the smallest is a model equivalent of the deep convection site after Pickart et al. (2002). The 1000-, 2000-, and 3000-m model isobaths are shown. (c) AR7W section of potential temperature in late March of year 8 in REBAT experiment.

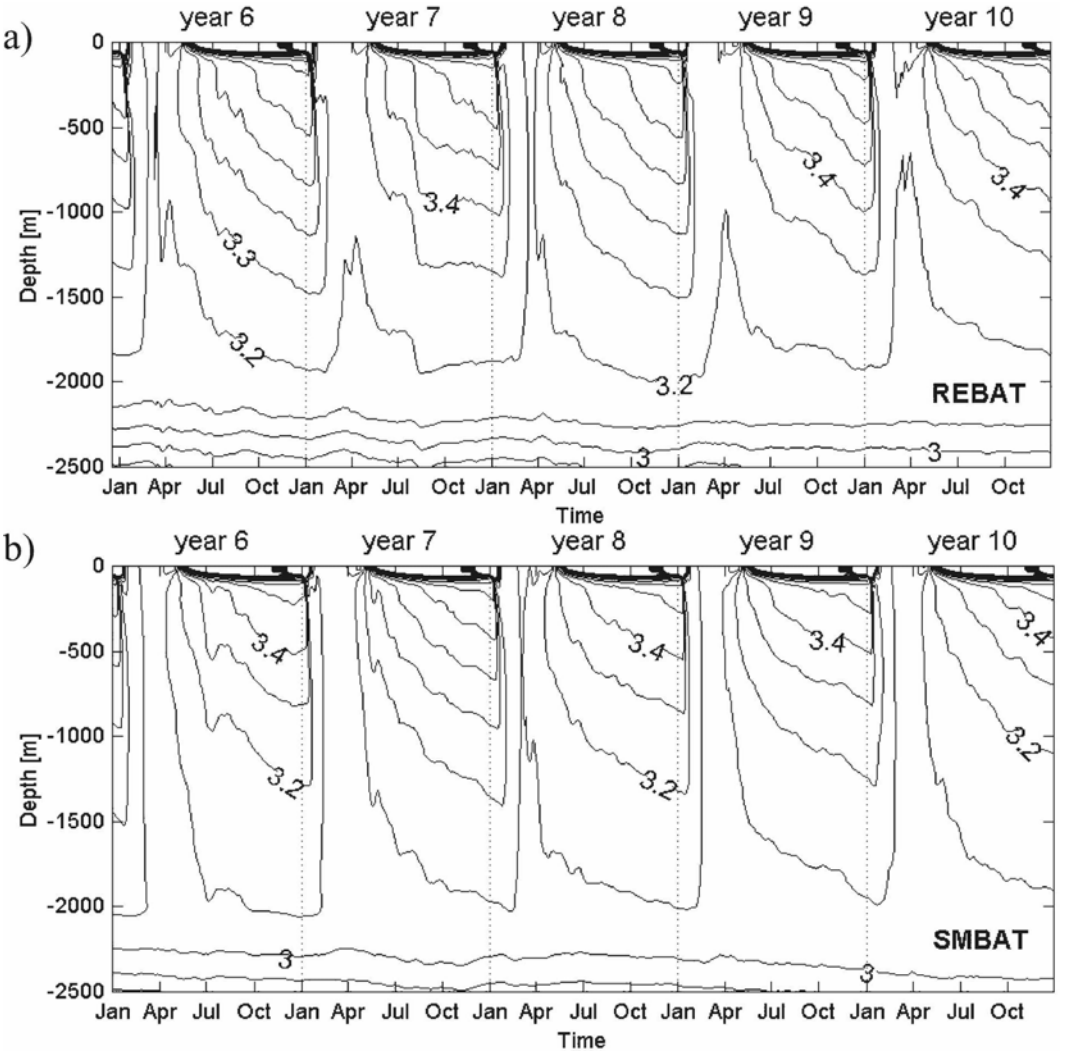

FIG. 9. Time evolution of the vertical temperature profile (°C) at the deep convection site (dashed circle in Fig. 8) in the (a) REBAT experiment and (b) SMBAT (no Irminger Rings).

potential temperature section in late March in Fig. 8c. It compares well with the winter 1997 section of Pickart et al. (2002) with a similar 200–300-km-wide pool of newly formed LSW. Note the mesoscale activity on the Greenland side of the basin, particularly the warm anomaly 300 km south of Greenland. It is one of the long-lived Irminger Rings, homogenized in its upper 500 m by the strong atmospheric cooling. Incidentally, a similar structure at almost the same place has also been mentioned by Pickart et al. (2002).

The seasonal cycle of the temperature associated with the alternating of winter convection and summer restratification at the location of the deep convection site (defined in Fig. 1) is well reproduced by the model (Fig. 9a). Subsurface stratification begins to build up in April and is fully established in January. The cycle of the convection depth is steady for the consecutive years, showing that the stratification is stable. This is a clear improvement compared to the coarser resolution NATL3 experiment in which Chanut (2003) finds no stratification associated with the summer warming (below the surface layer, temperatures remain homogeneous throughout the water column all year long). As a consequence, the convection depth continuously increases and reaches the bottom after 10 yr, as also shown by Willebrand et al. (2001) at the same ⅓° resolution.

4. Sources of eddy variability

The analysis presented in the previous section has demonstrated the ability of the embedded LAB15

model to simulate with a great deal of realism the important features of the mean and eddy circulation of the Labrador Sea, including the location and cycle of winter deep convection. The following section addresses the first objective of the study in an attempt to characterize the different sources of eddies in the model and the role of each at the deep convection site.

a. Irminger Rings

1) In the REBAT experiment

The Irminger Rings described by Eden and Böning (2002) and Katsman et al. (2004) are the numerous warm-core, energetic eddies (40–60 cm s^{-1} at the surface), about 45 km in diameter, found in the northern part of the Labrador Sea (see Figs. 8, 10). By visual inspection of relative vorticity anomalies near Cape Desolation (between 60° and 61°N) at about 200 m, we have selected all coherent eddies ejected from the boundary current for years 6 and 7 in REBAT. Then, these have been automatically tracked until the absolute value of their relative vorticity anomaly falls below 1×10^{-5} s^{-1}. The result is shown in Fig. 11. We identified 63 eddies shed from the boundary current. This agrees well with the 30 eddies per year estimated by Lilly et al. (2003). Most of the time eddies interact, merge, or get stalled in the vicinity of the boundary current. While most cyclones quickly collapse, there is a significant number of coherent anticyclones that are long lived (~2 yr), drift southwestward, and invade the northern part of the central Labrador Sea (north of 60°N). These are the Irminger Rings, well identified as strong negative anomalies in the vorticity field in Figs. 10a,b (about 10 rings can be identified in one snapshot of vorticity). If some IRs are finally captured by the boundary circulation on the western side of the basin, others propagate southward at about 3–4 cm s^{-1}, as hypothesized by Lilly et al. (2003) and Brandt et al. (2004), and get finally trapped at about 59°N, 52°W, where a secondary EKE maximum is seen (Fig. 6b). Interestingly, Prater (2002) also mentions such a localized anomaly near that particular point.

A detailed investigation of the Irminger Rings in REBAT simulation has been carried out by Mathiot (2004). The major findings of this unpublished study are summarized here. As is characteristic of all oceanic rings, model IRs have a core of negative potential vorticity (PV) surrounded by a ring of positive PV that acts as an effective barrier drastically limiting exchanges with surrounding waters. The evolution of their internal structure (temperature, salinity, and relative vorticity) is controlled by the vertical buoyancy flux during winter. Lateral exchanges with surrounding fluid, controlled by the numerical dissipation (quite low at this resolution), are weak. Because of this isolation, IRs are long lived (about 2 yr), which is a necessary condition for them to flux heat over long distances and to potentially contribute to the restratification of the deep convection site far from their region of generation at Cape Desolation.

However, very few model IRs go south of 58°N, where deep convection is observed (Fig. 11). Only one or two IRs per year are seen reaching the vicinity of OWS Bravo in the simulations. In addition, IRs crossing 58°N have generally seen their PV vertically homogenized by several convection events, as is the case for the IR located at 61°N, 54.5°W just north of the deep convection site in Fig. 8a: this eddy is vertically homogenized down to 1400 m, as indicated by the value of the mixed layer depth (in yellow in the figure). This is an important result regarding the role of IRs in the convection patch in the model. Because so few IRs are entering the patch and because the heat anomaly of those has been drastically reduced by several winter cooling events, the contribution of IRs to the seasonal restratification of the deep convection site is very likely marginal.

In a 5-yr record around the OWS Bravo mooring (1994–99), Lilly et al. (2003) found 12 anticyclonic Irminger Rings, which give a little bit more than two eddies per year—a little bit more than in our model study. Half of these have a characteristic double-core structure that could be the result, according to their analysis, of the merging of two eddies having different densities. Each core would correspond to the homogenization of a single eddy by convection. These eddies initially have a strong stratification, and we suspect, although this point was not raised by Lilly et al. (2003), that the lower core (between 1500 and 2000 m) is too deep to be created by a single convective event. It could be that most of them may have at least experienced two winters.

Our detailed investigation of the Irminger Rings in the present model simulations has shown that eddies that reach the deep convection site have a lifetime of about 2 yr. However, they do not exhibit such a double-core structure, a noticeable discrepancy with the observations by Lilly et al. (2003). IRs generally collapse after their second winter with mixed layer depths reaching about 2000 m at their center. One can speculate that in the case of moderate winter convection (our simulations correspond to a strong convection case), these probably could have lived longer and produced this characteristic structure. This dependency of the Irminger Rings' lifetime on the winter atmospheric forcing could also explain (in the limit of the numerical

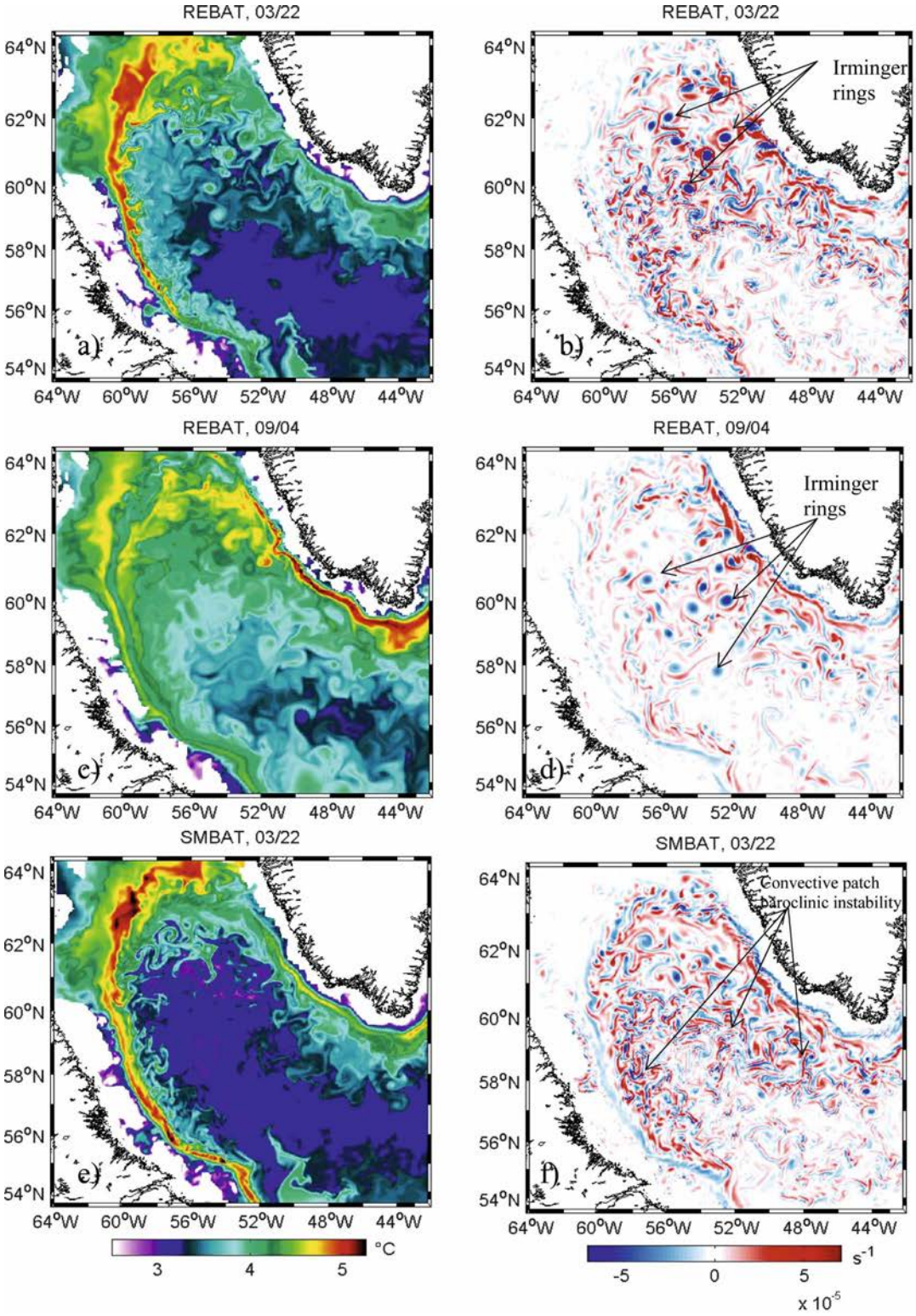

FIG. 10. Snapshots of (left) potential temperature and (right) relative vorticity at −182 m in the western part of the domain in March and September of year 8. (a)–(d) REBAT; (e),(f) SMBAT.

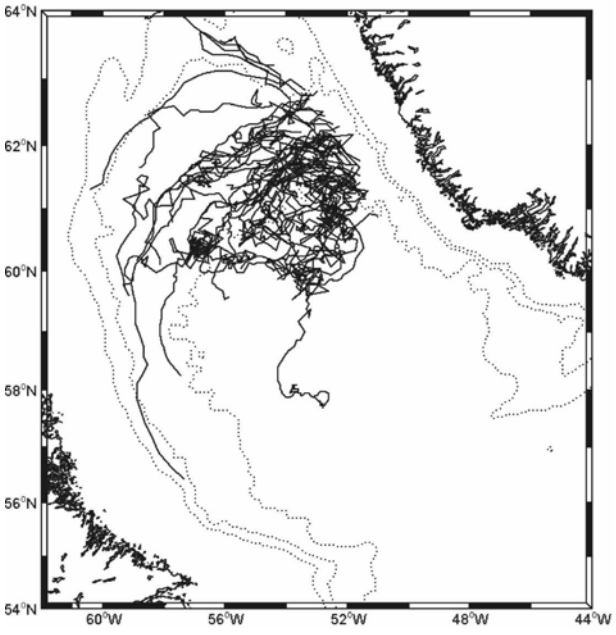

FIG. 11. Irminger Ring tracks for years 6 and 7 in the REBAT experiment. Dashed lines indicate the 1000-, 2000-, and 3000-m isobaths.

dissipation time scale) why more eddies were seen near the mooring in the observations than in the present model simulations.

2) IN THE SMBAT EXPERIMENT

The SMBAT experiment solely differs from the REBAT experiment by a smoother topography (see section 2). The most striking feature of this experiment, which is clearly seen in the instantaneous temperature and vorticity fields (Figs. 10e,f) as well as in the surface velocity field of Fig. 8b, is that it does not generate Irminger Rings. The EKE in SMBAT (Fig. 6c) is quite small within the IC, indicating a more stable rim current in this experiment, which supports the fact that certain small-scale details of the topography near Cape Desolation control the shear instability of the IC (Katsman et al. 2004). Indeed, the boundary current in SMBAT appears rather stable and continuous, nicely following the bathymetry all around the Labrador Basin (Fig. 8b), which seriously contrasts with the chaotic and turbulent aspect of the boundary current in REBAT (Fig. 8a). As a consequence of the absence of the IRs in SMBAT, the area of the interior Labrador Sea that is mixed by winter convection is significantly broader and extends in particular to the northern part of the sea (cf. Figs. 8a,b, 10a,c).

An important impact of the Irminger Rings on the thermodynamical seasonal cycle of the Labrador Sea is thus to limit the northward extent of the deep convection region and consequently the volume of LSW formed every winter. Because IRs are long lived and travel throughout the north-central Labrador Sea, their buoyant character extracted from the boundary current seriously limits deep convection and maintain in this region a significant stratification in the water column. Hence, they confine the region of deep convection to be farther south.

Considering water masses with mixed layer densities greater than 27.78 kg m^{-3} and west of 51°W, we calculated the volume of mixed dense water[1] in SMBAT to be 2.7×10^5 km^3, and 2.2×10^5 km^3 in REBAT. Thus, IRs can reduce by 20% the volume of deep water subject to convection (Clarke and Gascard 1983 give an estimate of 1.2×10^5 km^3).

b. Convective eddies and boundary current eddies

The temperature fields of experiment REBAT in March or September (Figs. 10a,c) exhibit turbulent structures other than IRs, in the form of meanders, eddies, and filaments (associated with small-scale relative vorticity structures, Figs. 10b,d), distributed on the offshore edges of the boundary current system. Upstream of Cape Desolation, the boundary current appears as a particularly important source of mesoscale activity with an almost permanent generation of eddies (most of them being anticyclones). These have an average diameter around 20–30 km and intermediate *T*–*S* properties between the interior and the boundary current. Animations of model outputs (http://meolipc.hmg.inpg.fr/Web/TEMP/JPO-Mov) show that they do not propagate in the basin's interior but merge or cascade to greater scales in a 200-km-wide area along the WGC. It seems that the altimeter does not sample this eddy activity. Perhaps evidence of such a signal can be found in the analysis of Advanced Microwave Scanning Radiometer for Earth Observing System (EOS; AMSR-E) passive microwave SST from Emery et al. (2006), where a warm temperature anomaly strip at 60°N is detected in winter.

Other small-scale relative vorticity structures, equally distributed in cyclonic and anticyclonic anomalies, are visible in the basin's interior but only for a short period of time in March–April (see Fig. 10b). Note that these are also found on the offshore side of the Labrador–Irminger Currents at the same time. Their geographical distribution, all along the rim of the convective patch (see Fig. 8), and their time of occur-

[1] Note that this does not represent the volume of newly formed LSW but rather the volume of deep water undergoing convection.

rence at the end of winter suggest that they are created by baroclinic instability triggered by the seasonal steepening of isopycnals.

The structures described above, akin to the boundary current eddies and convective eddies, respectively, discussed in the introduction, are also seen even more clearly in SMBAT (Figs. 10e,f). In fact, they are the dominant eddy signal in this simulation but are, however, far less energetic than IRs, as shown by the EKE maps of Fig. 6 (50–75 $cm^2\ s^{-2}$). By considering energy transfer rates, we have found (not presented here, see Chanut 2003), that EKE patterns associated with CEs and BCEs result, almost uniquely, from the conversion of potential energy and thus correspond to baroclinic instability. By contrast, the EKE maximum in REBAT principally appears to be the result of barotropic (horizontal shear) instability, as in the simulations of Eden and Böning (2002).

An important result of the above analysis has shown that in addition to IRs, the model simulates two other important sources of mesoscale eddies. One source corresponds to the boundary current eddies that are locally distributed and generated along the boundary current by weakly energetic instabilities. They are a way by which heat can also be fluxed from the boundary current into the Labrador Sea interior, as shown in the idealized model study of Spall (2004). Another source corresponds to the convective eddies that rapidly develop in early spring in the region of the interior Labrador Sea, where the deep penetrative convection occurs (the deep convection site) through baroclinic instability of steep isopycnals, as described in idealized model studies of open ocean convection (Jones and Marshall 1993, 1997).

c. Seasonal cycle of eddy variability

Figure 12 shows the time–latitude variations of monthly EKE zonally averaged between 48° and 55°W for both experiments and the TOPEX estimate of Lilly et al. (2003). In the REBAT experiment (Fig. 12b), IRs largely dominate EKE levels. Although it is active all year, the generation process of Irminger Rings shows a strong seasonal peak in winter (from December to March), which is not entirely linked to the convection cycle but is related to the seasonal variation of the circulation at the gyre scale. The southward propagation of rings (200 km in 3 months) seems to stop at 58°N (where a sharp decrease of EKE is found in Fig. 12b), in agreement with the individual eddy tracks in Fig. 11. The southward propagation of IRs is less marked in the model than in observations. As discussed in the previous subsection, this could be explained by the impact of the atmospheric forcing on the strength of Irminger

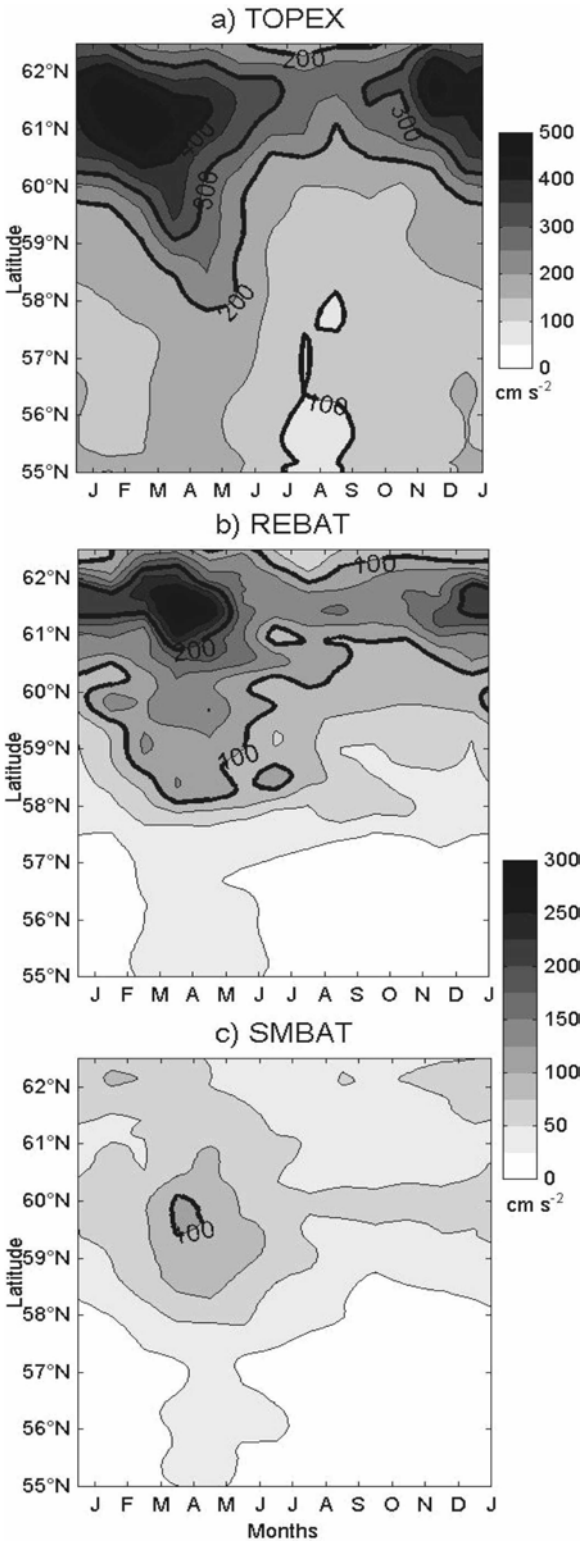

FIG. 12. (a) Monthly mean EKE deduced from TOPEX satellite altimeter between 1994 and 2000 (Lilly et al. 2003), zonally averaged between 55° and 48°W (see box on Fig. 6a). (b), (c) Same as (a), but for experiments REBAT and SMBAT, respectively. CI is 50 $cm^2\ s^{-2}$ for (a) and 25 $cm^2\ s^{-2}$ for (b) and (c).

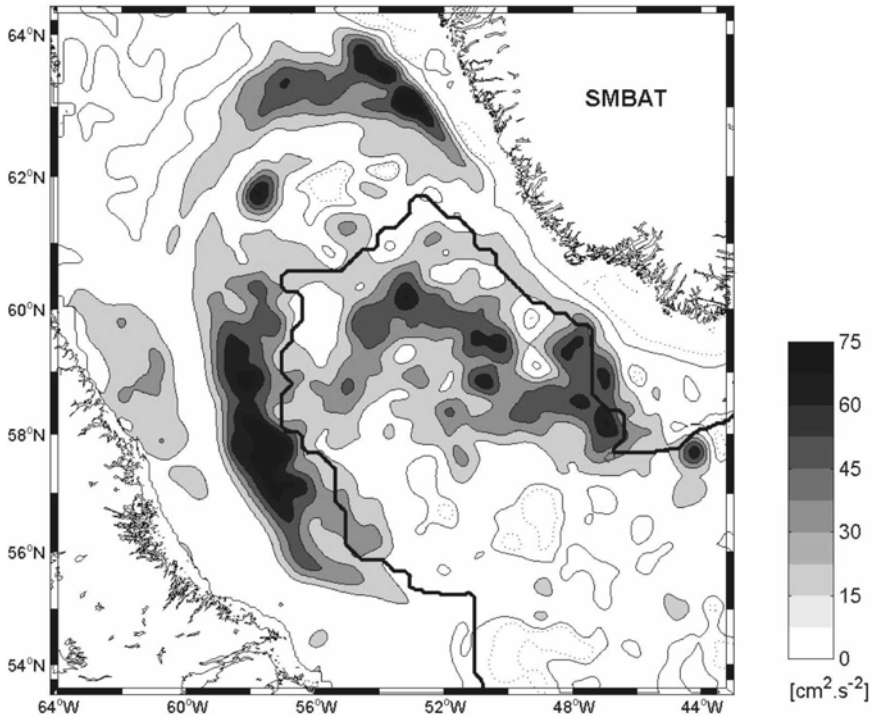

FIG. 13. March EKE anomaly at about 100 m in the SMBAT experiment.

Rings in the present simulations. Another possibility is that the increase of lateral density gradients due to heat loss also speeds up the BCS, making the localized WGC instability more continuous. Support for these hypotheses can be found in the analysis of the interannual variability of the WGC instability discussed in Brandt et al. (2004). They show that the seasonal cycle WGC was greatly reduced in the early '90s [e.g., under harsh wintertime conditions (see their Fig. 8b)]. It seems that no clear propagation south of 60°N occurred during this time period, while it was particularly obvious in 1997–2000 when winter heat losses were moderate.

With no Irminger Rings (experiment SMBAT; Fig. 12c), no apparent seasonal cycle in the core of the BCS north of 61°N can be noticed. This proves the stabilizing effect of the topographic smoothing. A peak of energy (100 $cm^2\ s^{-2}$) is seen in late March at about 59°N, which corresponds to the small-scale turbulence (i.e., the convective and boundary current eddies) in Fig. 10f (see also March EKE anomaly in Fig. 13). This signal almost instantaneously invades the basin interior and quickly vanishes in May as the available potential energy input has ceased. Interestingly, there is a hint of a similar phenomenon in the observed cycle of Fig. 12a, although according to Lilly et al. (2003) such anomalies would be too weak to be captured by the altimeter. Perhaps more convincing evidence of such a signal in observations can be found in the mooring analysis of Lilly et al. (2003). They indeed detect a very brief increase of "noneddy" events in March–April. Note that the sudden EKE increase in the model also involves the offshore sides of the WGC–IC currents (Fig. 13), making the scenario finally less simple than the breakup of an isolated convective patch.

The dominant eddy seasonal signal in the SMBAT experiment thus appears intimately linked to winter deep convection, which feeds the baroclinic instability of the boundary current system but also triggers a sudden energization of the whole interior by a burst of baroclinic instability around the convective patch in early spring. Note that this burst of energy coincides with the fast restratification of the convection site shown in Fig. 9. The overall picture is thus consistent with a major contribution of the CEs to the restratification process, as in simulations of open ocean deep convection with idealized model setup (Jones and Marshall 1997).

As demonstrated in the next section, the SMBAT experiment sheds light on low-EKE (yet fundamental) processes for the heat transfer in the Labrador Sea interior. These processes are also at work in REBAT, as shown in the vorticity snapshots of Fig. 10, but they are more difficult to characterize because the variability is dominated by the more energetic IRs.

5. Interior eddy-induced heat equilibration

In this section, the role of eddy mixing on the heat budget of the quasi-equilibrated state is examined. Because we have shown in the previous section that Irminger Ring generation could be suppressed in the SMBAT experiment, differences between SMBAT and REBAT will serve to quantify their importance and to highlight the role of lower-energy processes that are difficult to sort out in the presence of IRs.

a. Heat content equilibration

We consider here the evolution of the heat content in the region of the interior Labrador Sea, where maximum deep convection occurs. This region is defined as the cylinder centered at 58.6°N, 52.5°W of radius R = 250 km and depth h = 2000 m (see Fig. 8). This region thus excludes boundary currents and bottom layers but is deep enough to account for most of the effect of surface forcing (mixed layer depths in the interior hardly reach 2000 m after 8 yr; see Fig. 8). The column heat content per unit area, H, is defined as

$$H = \rho_0 C_p \frac{1}{\pi R^2} \int\int\int_V T \, dv, \qquad (2)$$

where C_p = 4000 J kg^{-1} °C^{-1} is the specific heat of water, ρ_0 = 1027 kg m^{-3} is a reference density, T is the model potential temperature, and V is the volume of the cylinder.

Time series of this quantity from the beginning of the simulations are shown in Fig. 14a and are compared with the time-integrated surface forcing over this area. The effective model forcing, which is almost identical for both REBAT and SMBAT, is in average extracting about 2.5 GJ m^{-2} yr^{-1} from the water column (equivalent to an averaged heat loss of 80 W m^{-2}). While still in the range of the observed annual heat loss, this value seems more representative of intense convection years [from recalibrated National Centers for Environmental Prediction (NCEP) fluxes, Straneo (2006) estimates a mean annual heat loss of 28.5 W m^{-2}]. Despite this considerable heat loss, the heat content, which shows a small increase during the first 4 yr, remains in a quasi-steady cycle for the rest of the integration. This implies a quasi compensation of the surface cooling by some lateral input of heat.

Lateral advective fluxes, shown in Fig. 14b, have been calculated by removing the forcing contribution to the column change (this "residual" estimate of the lateral advective fluxes includes the contribution of the vertical flux at 2000 m and the parameterized diffusion, the contribution of which is negligible as shown in Fig. 15). It appears that the thermal equilibration is indeed governed by the spinup of lateral fluxes, which progressively matches surface fluxes that are almost steady after a couple of years.

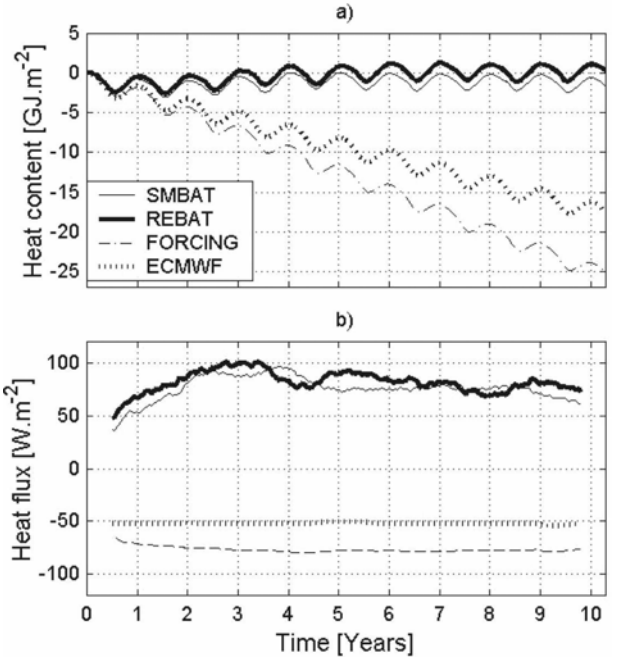

FIG. 14. Heat budget of the basin interior, defined by the largest circle on Fig. 7. (a) Thick (thin) continuous lines: heat content evolution in the top 2000 m in REBAT (SMBAT), respectively; dashed lines: Time-integrated model surface forcing; dotted line: time-integrated original ECMWF forcing. The difference between model and ECMWF is due to the contribution of the flux correction in the forcing formulation. (b) Thick (thin) continuous lines: lateral advective fluxes in the 2000-m water column in REBAT (SMBAT), respectively; discontinuous dashed–dotted lines: model (ECMWF) surface heat fluxes. Data were filtered with a 1-yr boxcar window. Note that year 0 starts in mid-September, the beginning of the cooling period.

What is puzzling about the above results is that the greatly enhanced eddy activity in the REBAT experiment yields a relatively small change in the interior heat content evolution compared to the SMBAT experiment. In particular, the time for eddy and mean advection to reach a quasi equilibration with the surface forcing is similar (3–4 yr). After 10 yr, the heat content difference between the two experiments is approximately 1.2 GJ m^{-2} (in favor of REBAT, which is warmer), equivalent to a constant heat flux of only 4 W m^{-2} (fairly small compared to the 80 W m^{-2} required to balance the surface heat loss). From temperature contours in Fig. 16, differences between experiments are essentially located near Cape Desolation, although the warming has propagated in the whole basin. As far as eddy fluxes from the boundary current may be con-

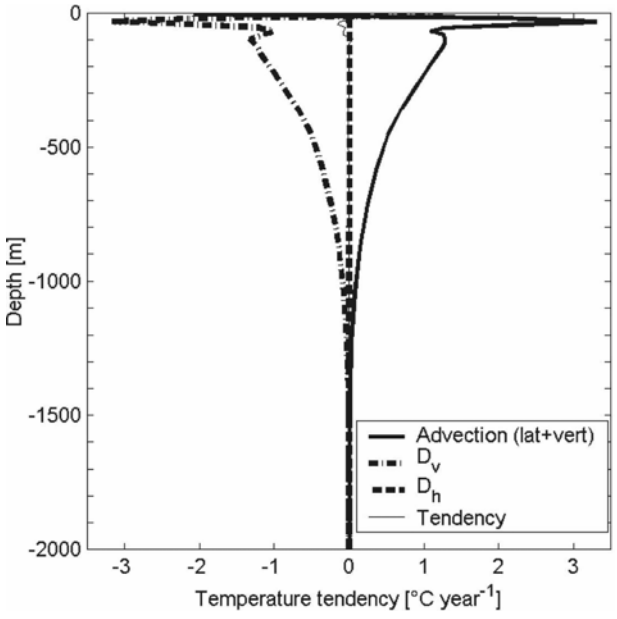

FIG. 15. Contribution of the various terms of the temperature equation to the annual budget in the interior region (large circle in Fig. 7) for the REBAT experiment (the picture is almost identical for SMBAT).

cerned, however, it is important to relate the interior's temperature and density changes to the lateral gradients. Taking along the AR7W section mean profiles between 400 and 600 km from the Labrador coast for the interior and for depths lower than 2500 m over the Greenland slope for the Irminger–WGC, we found a substantial increase of the mean temperature gradients from $\Delta T = 1.0$°C in REBAT to $\Delta T = 1.2$°C in SMBAT experiments. On the other hand, lateral density gradients do not change much between experiments, the interior being saltier in REBAT than in SMBAT, which partially compensates for the warming.

b. Heat budget

1) ANNUAL MEAN BUDGET

To investigate more precisely the heat budget in the basin interior, we examine here the different terms in the temperature equation

$$\frac{\partial T}{\partial t} = -\boldsymbol{\nabla} \cdot (\mathbf{u}T) - \frac{\partial (wT)}{\partial z} + D_h + D_v, \qquad (3)$$

where $\mathbf{u}$ is the horizontal velocity vector, w is the vertical velocity, and D_h and D_v are the horizontal and vertical diffusion, respectively (this latter term also includes the forcing). These terms have been explicitly calculated during the last 5 yr of each experiment, and their average in the interior is represented in Fig. 15 for the REBAT experiment (the picture for SMBAT being almost identical). As expected from the above discussion, the tendency is small compared to the magnitude of other terms. Down to approximately 2000 m, which is approximately the maximum depth where deep convection penetrates, there is a balance between vertical mixing and advection terms, while horizontal diffusion is an order of magnitude smaller. Note that lateral advection tends to warm the whole column, although Straneo (2006) found that lateral advection should be negative in the 100-m-thick surface layer. This discrepancy may be a consequence of the cold surface boundary currents trapped on the shelf break in our simulations.

Advective terms in (3) are further partitioned into mean and fluctuating components of the resolved velocity $\mathbf{u}$ and temperature T. This avoids any possible confusion with parameterized unresolved terms:

$$\boldsymbol{\nabla} \cdot (\mathbf{u}T) + \frac{\partial (wT)}{\partial z} = \boldsymbol{\nabla} \cdot (\overline{\mathbf{u}}\,\overline{T}) + \frac{\partial (\overline{w}\,\overline{T})}{\partial z} + \boldsymbol{\nabla} \cdot (\overline{\mathbf{u}'T'}) + \frac{\partial (\overline{w'T'})}{\partial z}. \qquad (4)$$

The overbar represents a 5-yr mean and primes represent deviations from this average. The vertically integrated (between 180 and 1300 m) eddy heat flux (the $\overline{\mathbf{u}'T'}$ term) is shown in Fig. 16. The pattern of the eddy heat flux in SMBAT (Fig. 16b) is entirely due to CEs and BCEs. In view of the analysis of the vorticity fields of Fig. 10 and of the March eddy kinetic energy map of Fig. 13, the distribution of the eddy flux along the rim of the boundary current (here defined as the 4°C isotherm line) can be attributed to the BCEs, and the maximum eddy flux in the central Labrador Sea can be attributed to the CEs. In REBAT (Fig. 16a), the Irminger Rings' shedding induces a clear and significant increase in eddy heat flux near Cape Desolation, but elsewhere the pattern of eddy fluxes is similar to SMBAT. Eddy heat fluxes carry heat from the boundary currents to the interior and are generally greater on the Greenland side. In view of the mean temperature contours as they appear in Fig. 16, there is an obvious downgradient relationship almost everywhere. By analogy with Fickian diffusion, the downgradient component of eddy fluxes $\overline{u'T'}_{\perp}$ can be written as a function of the mean temperature gradient:

$$\overline{u'T'}_{\perp} = -K(\boldsymbol{\nabla}\overline{T} \cdot \boldsymbol{\nabla}\overline{T})^{1/2} \qquad (5)$$

where K is an eddy downgradient diffusivity given by

$$K = -\frac{\overline{\mathbf{u}'T'} \cdot \boldsymbol{\nabla}\overline{T}}{\boldsymbol{\nabla}\overline{T} \cdot \boldsymbol{\nabla}\overline{T}}. \qquad (6)$$

By excluding places of low gradient of $\overline{T}$ and using seasonal averages, we found a coherent pattern with

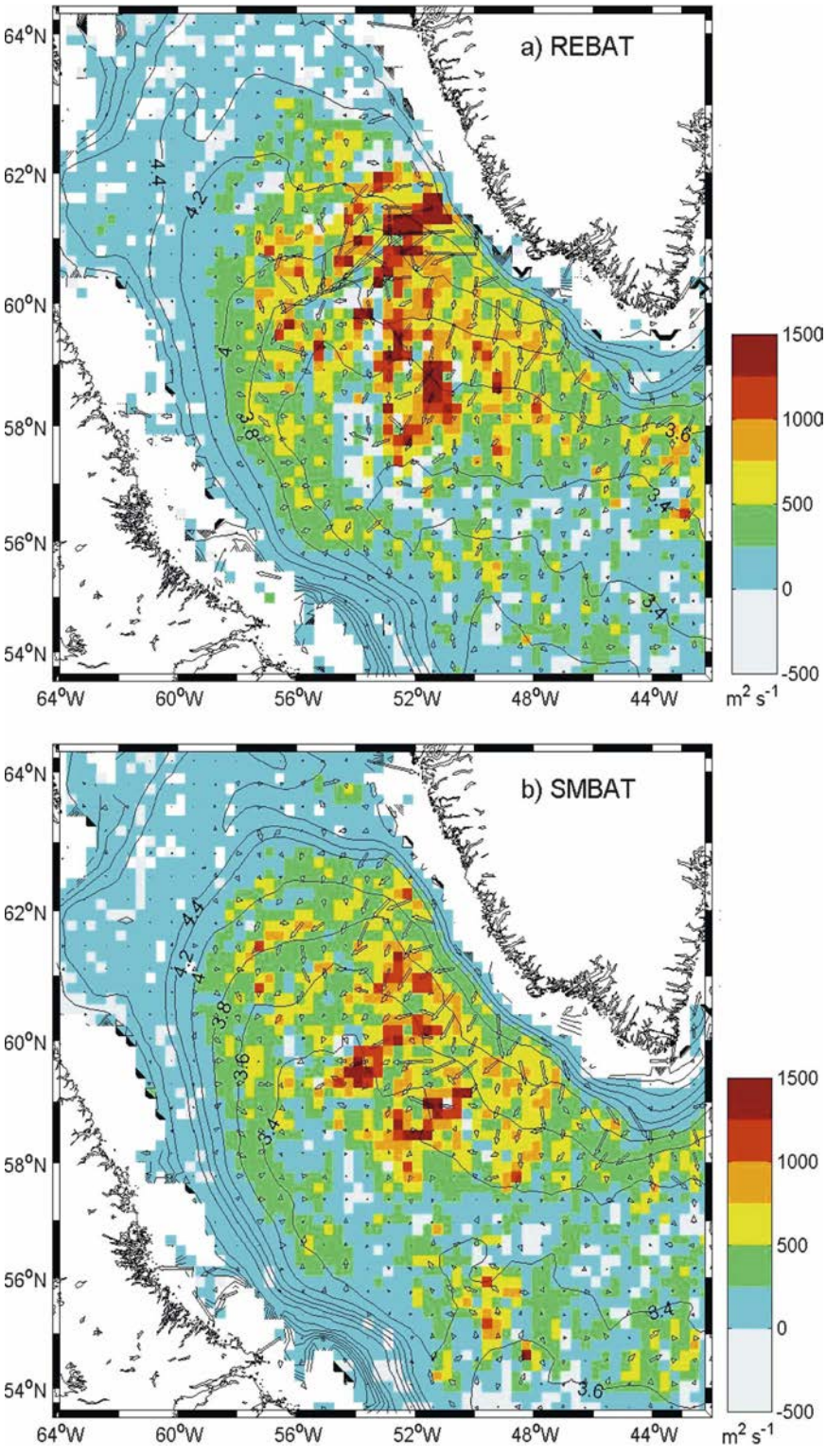

FIG. 16. Mean downgradient eddy diffusivity of temperature averaged between 180 and 1300 m and by 1° bins. Contour lines show the mean temperature (CI = 0.2°C), vectors show the lateral eddy flux of temperature, and colors indicate the value of the downgradient eddy diffusivity coefficient estimated from the eddy heat flux in the (a) REBAT experiment and (b) SMBAT.

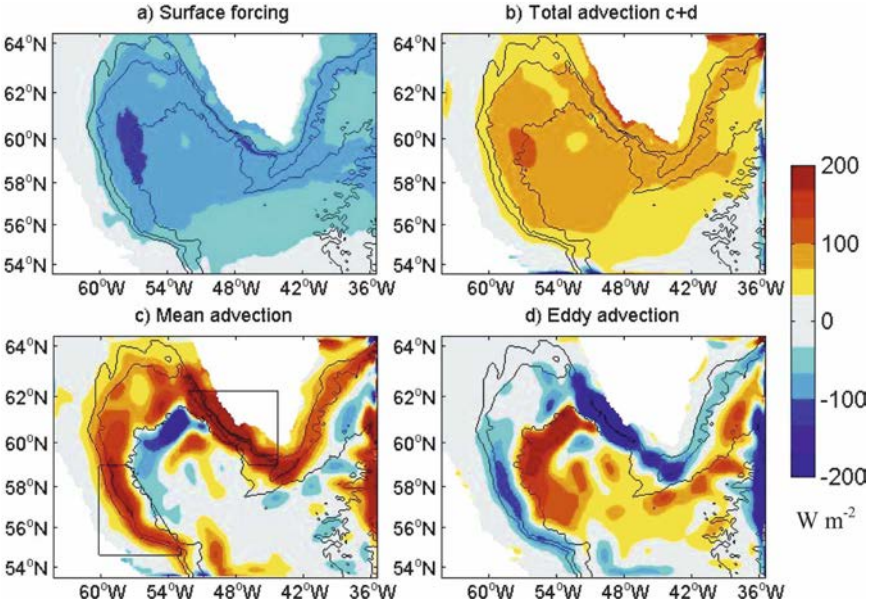

FIG. 17. Depth-integrated heat budget (W m^{-2}) in REBAT (a 31-point Hanning window has been applied prior to plotting). The various terms of the budget are (a) surface fluxes, (b) total advection (mean + eddy), (c) mean advection, and (d) eddy advection. Positive (negative) values mean local temperature increase(decrease). The 1000-, 2000-, and 3000-m model isobaths are shown. Boxes indicate the WGC and LC areas used for the budget of Table 2.

few negative values. The vertically averaged value of K between 180 and 1300 m is shown in Fig. 16 for each experiment. It strongly recalls the EKE geographical distribution. In the REBAT experiment, it reaches 1500 $m^2\,s^{-1}$ near Cape Desolation, but there is also a strip of enhanced diffusivities (around 800 $m^2\,s^{-1}$) along the WGC and the LC in both cases (the BCEs). The picture in the REBAT experiment is finally in general agreement for both the distribution and magnitudes with the Lagragian estimate of Straneo et al. (2003). However, one has to keep in mind that these diagnostics are certainly biased by the unavoidable presence of rotational fluxes.

The terms on the right-hand side of (3) have been calculated diagnostically and vertically integrated to the bottom. Because of the rigid-lid assumption, the integral of vertical advection terms vanishes. Thus, it allows one to evaluate the annual balance between lateral advection of heat by the mean flow, eddies, and the surface heat flux. The result is shown in Fig. 17 for the REBAT experiment only, but the picture for the SMBAT experiment is very similar, so the comments made below hold for both experiments. Negative (positive) values mean a local temperature decrease (increase). Because the system has reached a quasi-steady state, the total advection (mean + eddy; Fig. 17b) balances the surface heat loss (Fig. 17a) over the entire basin. Quantitative results for heat budget in different areas of the Labrador Basin are summarized in Table 2. First considering the total LAB15 refined-grid domain (last line

TABLE 2. Area-averaged components in the annual heat budget (W m^{-2}). The "residual" term includes horizontal dissipation and the trend. The WGC box and LC box are shown in Fig. 17.

Location	Mean advection $-\rho_0 C_p \tau \int_Z \nabla\cdot(\bar{\mathbf{u}}\,\bar{T})\,dz$ REBAT/SMBAT	Eddy advection $-\rho_0 C_p \int_Z \nabla\cdot(\overline{\mathbf{u}'T'})\,dz$ REBAT/SMBAT	Surface flux $\overline{Q}$ REBAT/SMBAT	Residual REBAT/SMBAT
WGC box	+488/+320	−412/−246	−78/−76	−2/−2
LC box	+90/+71	−36/−20	−55/−53	−1/−2
Interior (largest circle in Fig. 8a)	−12/+15	+96/+61	−79/−78	+5/−2
Total refined grid domain	+53/+45	−1/+2	−57/−54	−5/−7

in Table 2), it appears that the lateral eddy advection of heat through open boundaries is negligible (−1 W m^{-2}), so the heat required to balance the surface heat loss to the atmosphere in the whole domain (−57 W m^{-2}) is supplied by the large-scale mean circulation of the boundary currents (53 W m^{-2}). It is then redistributed to the interior almost exclusively by eddies: the average contribution of the mean circulation to the basin interior heat budget is almost negligible (−12 W m^{-2}) while eddy advection largely dominates (+96 W m^{-2}). The heat budget is qualitatively similar in SMBAT, and the same conclusion holds that the heat fluxed by eddies is sufficient to achieve a realistic quasi equilibrium over a time scale of a few years. It is worth noting that the heat carried by eddies originates all along the boundary current system (e.g., the large eddy heat flux out from the WGC and the LC boxes), not only from where Irminger Rings are shed. It thus makes the long-term eddy-induced equilibration scenario finally similar to the idealized experiments of Spall (2004), where no IRs were generated.

2) Seasonal Cycle

In a study of the seasonal cycle of the central Labrador Sea, Straneo (2006) shows that for convective years only, the restratification phase has two distinct stages: after the cooling ceases in late March, there is a 2- to 3-month quick warming period of the column followed by a slower adjustment until the next convective event. She argues that the first stage is caused by a violent reorganization of the convected waters in the interior (and as a matter of fact does not occur for nonconvective years), while the second is a slower exchange with the boundary currents. Our experiments confirm this. From the time evolution of temperature profiles in the deep convection area shown in Fig. 9, it is clear that there is a quicker warming of the column between April and July. This can be enlightened by considering the time evolution of the monthly lateral flux through the interior in Fig. 18. It shows that the lateral heat flux increases between January and July with a strong peak up to 140 W m^{-2} in March–April. This picture agrees well with the mean seasonal cycle derived by Straneo (2006) from the combination of (profiling) autonomous Lagrangian circulation explorer [(P)ALACE] floats/Bravo mooring temperature profiles and recalibrated NCEP fluxes.

From Fig. 18, it appears that the time evolution of fluxes is finally very similar in both experiments as is the evolution of temperature shown in Fig. 9. Obviously, in the SMBAT experiment, the peak is related to the sudden energization described in section 4, while in the REBAT experiment the WGC instability increase

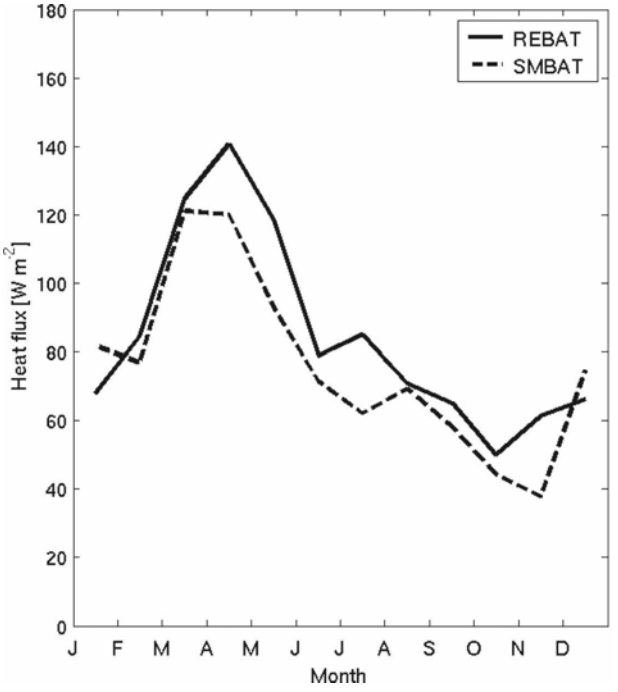

Fig. 18. Monthly lateral heat flux in the interior (W m^{-2}) averaged for years 6 to 10.

may also have an effect. Interestingly, in the deep convection area, we also find in both experiments a peak up to 200 W m^{-2} at the same time (not shown), which coincides with the occurrence of the small-scale vorticity structures associated with the CEs in Fig. 10. Such coincident signals cannot be explained by an advective turbulent process from the boundary current. Thus, it is likely that in both experiments the heat flux peak is caused by the baroclinic instability that involves the whole interior.

6. Summary and conclusions

The role of mesoscale ocean turbulence in the cycle of open ocean deep convection in the Labrador Sea has been examined in a high-resolution regional model. Two related foci are the annual heat budget of the basin and the processes of restratification. The experimental design extends previous idealized studies to an eddy-resolving resolution with realistic geometry, topography, forcing, and interaction with the North Atlantic. The Labrador Sea domain is imbedded in an eddy-permitting North Atlantic Ocean, using a state-of-the-art primitive equation ocean model and a grid-refinement package. The model solution in the fine-grid Labrador Sea is analyzed from a 10-yr-long integration, during which the model is driven by a cli-

matological monthly forcing. The simulated boundary current system, eddy fields, and deep convection cycle all compare well with observations, despite certain biases, especially in the thermohaline properties, which are mainly due to the large-scale North Atlantic model.

In spite of a large net annual surface heat loss, the modeled Labrador Sea converges to a stable cycle of deep convection and a thermal quasi equilibrium. The basin-wide surface heat loss is balanced by mean advection, with the currents entering south of Greenland carrying more heat than exits with the Labrador Current in the west. However, in the central basin, mean advection is almost negligible, and the surface loss is balanced by the eddy flux of heat from the BCS. This result is in general accord with more idealized models (Jones and Marshall 1997; Spall 2004; Katsman et al. 2004), but the more realistic model reveals a more complex role played by the mesoscale turbulence. Most notably, there are three distinct eddy types, as distinguished by source region, generation mechanism, and dynamics. Each has a unique contribution to the heat budget of the central Labrador Sea and hence to the cycle of deep convection.

The role played by Irminger Rings is revealed by the REBAT experiment and its difference from SMBAT. As expected from Eden and Böning (2002), topographic instability off Cape Desolation generates IRs, which are the source of high EKE levels seen north of about 60°N in satellite altimetry. Like all ocean rings, their peculiar potential vorticity structure insulates them from surrounding waters. Therefore, they are primarily modified by surface exchanges with the atmosphere, especially heat loss. In REBAT, IRs are confined to the Labrador Sea north of about 58°N, where their presence and this exchange insulates the ambient ocean from the surface buoyancy loss needed to precondition the ocean for deep convective mixing. A critical role of IRs is therefore to limit the production of LSW, by restricting the northward extension of deep convection. This control and the large interannual variability of the associated WGC–IC instability (Brandt et al. 2004) make it possible for IRs to have an important role in the variability of LSW production. However, in contrast to Katsman et al. (2004), we suspect that their *direct* contribution to the restratification of the deep mixed layers is likely to be moderate. Although we did not calculate this contribution explicitly, very few IRs enter the deep convection site, and those that do have experienced two winters of vertical mixing, thus representing a small heat content anomaly.

Boundary current eddies are associated with distributed, weakly energetic instabilities all along the BCS. They are similar to the idealized eddies studied by Spall (2004) and are the major source of EKE along the Labrador coast as well as the Greenland coast south of Cape Desolation. Emery et al. (2006) pointed out the existence of a *distributed* warm anomaly along the WGC–Irminger Currents in satellite SST data in agreement with such a signal. They flux heat from the BCS to the interior by propagating offshore of both coasts and mixing with the ambient ocean. Thus, in a somewhat different way, they also tend to thwart preconditioning and limit LSW production. In the north, they act in concert with the IRs, and their lateral mixing could be important even though the very energetic IRs mask their weaker energy field (Böning and Eden 2002). Farther south, they appear to transport sufficient heat to overcome the surface cooling everywhere, except for a small region toward the west of the central Labrador Sea. This region is the deep convection site of Fig. 1, and its size and location are well represented in the model. It is near the Labrador coast, because BCEs from the Labrador Current do not flux heat as efficiently as those from the Greenland side. If they did, ocean deep convection would likely not occur in the Labrador Sea. It is possible to further speculate that a narrower basin, or more topographic instabilities due to changing sea levels, for example, could cause a similar result.

The final piece of the interior heat budget puzzle is the contribution of convective eddies. They are generated through baroclinic instability of steep isopycnals that develop during late winter deep convective mixing events. Thus, they produce a distinct seasonal cycle in EKE with a peak in April. CEs are born in the vicinity of the deep convection site and are therefore very effective at transporting heat into the convective patch. Thus, they are a major player in the early stages of restratification throughout the patch. However, they require horizontal temperature gradients, which are supplied by the BCEs. Therefore, CEs can be seen as efficient final seasonal relays in fluxing heat extracted from the boundary current system, through the BCEs, into the deep convection site. The restratification continues to strengthen, both near the surface due to solar heating and possibly at depth due to BCEs. It sets many of the requirements for preconditioning the ocean for the next winter's deep convection.

In SMBAT, the topography was smoothed to the point that IRs were no longer shed offshore of Cape Desolation. Assuming other effects of smoothing are much less important, the role of IRs can be isolated from the other eddy types by comparing REBAT and SMBAT results. A comparative analysis of the turbulent mesoscale fluxes indicates that the roles of BCEs and CEs are qualitatively the same in both experiments

and that the presence of IRs is not necessary to achieve a quasi equilibrium in the interior Labrador Sea. However, in the SMBAT equilibrium, the deep convection site is greatly expanded toward the north, suggesting that the BCEs alone are insufficient to prevent the surface cooling from adequately preconditioning a much larger area. Without IRs, this expanded region continues to cool in winter until CEs begin to flux heat into the site following their generation in response to a deep convective mixing event.

More dramatic responses would be expected if there were either no BCEs or CEs, as might be the case in a coarse-resolution ocean model with a deficient eddy parameterization. With no heat supply from the BCS, there could be widespread cooling of the central basin, and there would be no supply of heat for CEs to restratify the convective patches until they bordered the BCS. Any quasi equilibrium would be expected to be very different and involve sea ice in the central basin. If, instead, only CEs were missing, restratification would be limited to whatever the surface heating and lateral fluxes from BCEs could provide. A likely scenario would be deeper convective overturning each year until it reached the ocean bottom.

Although our model setup is realistic and the major observed mean and eddy features of the circulation in the Labrador Sea are well represented, some caution is due when applying the results to the real ocean. The simulation is over 10 consecutive years of strong convection (annual atmospheric heat loss of -80 W m^{-2}). The impact on IRs could be significant, because air–sea fluxes are the major cause of their modification. In periods of weak convection, IRs would likely retain the heat extracted from the BCS longer and contribute to the thermal equilibrium of the interior differently. Moreover, despite its high resolution (4 km), the embedded model is still significantly more diffusive than nature, which may impact the life cycle of long-lived eddies such as IRs.

Acknowledgments. The authors thank Jonathan Lilly for providing the altimeter data and Lu Youyu for the climatological dataset. The MODIS SST data were obtained from the Physical Oceanography Distributed Active Archive Center (PO.DAAC) at the NASA Jet Propulsion Laboratory, Pasadena, CA (http://podaac.jpl.nasa.gov).

This work is part of the Ph.D. thesis of Jérôme Chanut funded by the Centre National de la Recherche Scientifique (CNRS) and the Direction Générale de l'Armement (DGA). General support from the Institut National des Sciences de l'Univers (INSU) and CNRS are acknowledged. Visitor support was provided by the Advanced Study Program at the National Center for Atmospheric Research. Computations presented in this study were carried out at Institut du Développement des Ressources en Informatique Scientifique (IDRIS). The study presented here was carried out in the framework of the CLIPPER project, with the support of the Groupe Mission Mercator Coriolis (GMMC) and a specific contribution from Service Hydrographique de la Marine (SHOM) to support the visit of W. Large at Laboratoire des Ecoulements Géophysiques et Industriels (LEGI) in Grenoble.

APPENDIX

The Embedding Procedure

The coupling between the 1/3° North Atlantic grid and the fine 1/15° Labrador Sea grid is achieved with the AGRIF package (Adaptive Grid Refinement In FORTRAN, Blayo and Debreu 1999; Debreu et al. 2005). More information about the package can be found online (http://www-lmc.imag.fr/IDOPT/AGRIF/index.html). AGRIF is an ensemble of FORTRAN 90 routines for implementing adaptive grid refinement within a finite difference numerical model. The core of this package lies in the use of pointers, which allows a single variable name to address both the value of a coarse-grid model (CGM, here NATL3) and a fine-grid model (FGM, here LAB15). It thus minimizes changes in the original code, essentially restrained to the call of interpolation procedures when a boundary value is necessary or for surface forcing fields. Although only a two-level static-grid embedding is performed in this study, AGRIF is designed to manage an arbitrary number of embedding levels with refined areas moving in the course of integration (Debreu et al. 2005).

AGRIF handles the time stepping order between the grids as follows: because the time step of the FGM has to be divided by the refinement factor compared to the CGM's to satisfy the numerical CFL criterion, successive time steps (five in our case) are performed on the FGM for every CGM step. At the refined-grid interface, boundary conditions are provided by a linear interpolation (spatial and temporal) of the CGM fields (temperature, salinity, velocities, and the barotropic streamfunction). At this stage, a feedback of the fine-grid fields on the coarse-grid field is performed by replacing CGM values at overlapping points inside the refined area by a volume average of the new FGM values (for the present study, the average has been performed over 5×5 points at each vertical level). In this case, the interaction between the two grids is "two ways." Otherwise, when the coarse grid is not updated

with the fine-grid solution, the coarse-grid solution remains independent of the refinement: this is "one-way" embedding. In the following, the two-way approach has been used, essentially to ensure a better connection between the grids. Tests with a one-way embedding system indeed show that some distortion arises at the refined boundary for long (several years) integrations. These are much reduced with a two-way interaction, as shown by Fox and Maskell (1996). Moreover, while all the results in the following concern the refined area, our experiments can be used in further studies to investigate the large-scale impact of local grid refinement. Finally, a thin layer of enhanced Laplacian viscosity has been added adjacent to the limit of the fined/coarse domains to damp occasional oscillations and to dissipate turbulent structures smaller than a coarse-grid box. Viscosity and diffusivity increase (as a sine) up to 300 and 150 $m^2 s^{-1}$, respectively, over the last 11 grid points of the fine-grid domain. Note that NATL3 and LAB15 have approximately the same number of points (Table 1). In terms of computing time, it follows that the North Atlantic model represents only ⅙ of the total (interpolation overhead is negligible).

REFERENCES

Barnier, B., 1998: Forcing the ocean. *Ocean Modeling and Parameterization,* E. P. Chassignet and J. Verron, Eds., Kluwer Academic, 45–80.

——, L. Siefridt, and P. Marchesiello, 1995: Thermal forcing for a global ocean circulation model using a three-year climatology of ECMWF analyses. *J. Mar. Syst.,* **6,** 363–380.

Blanke, B., and P. Delecluse, 1993: Variability of the tropical Atlantic Ocean simulated by a general circulation model with two different mixed-layer physics. *J. Phys. Oceanogr.,* **23,** 1363–1388.

Blayo, E., and L. Debreu, 1999: Adaptative mesh refinement for finite-difference ocean models: First experiments. *J. Phys. Oceanogr.,* **29,** 1239–1250.

Brandt, P., F. A. Schott, A. Funk, and C. S. Martins, 2004: Seasonal to interannual variability of the eddy field in the Labrador Sea from satellite altimetry. *J. Geophys. Res.,* **109,** C02028, doi:10.1029/2002JC001551.

Chanut, J., 2003: Paramétrisation de la re-stratification après convection profonde en mer du Labrador. Ph.D. thesis, Joseph Fourier University, 185 pp.

Clarke, R. A., and J.-C. Gascard, 1983: The formation of Labrador Sea Water. Part I: Large-scale processes. *J. Phys. Oceanogr.,* **13,** 1764–1778.

Cuny, J., P. Rhines, S. Niiler, and S. Bacon, 2002: Labrador Sea boundary currents and the fate of the Irminger Sea Water. *J. Phys. Oceanogr.,* **32,** 627–647.

Debreu, L., E. Blayo, and B. Barnier, 2005: A general adaptive multi-resolution approach to ocean modelling: Experiments in a primitive equation model of the North Atlantic. *Adaptive Mesh Refinement: Theory and Applications,* T. Plewa, T. Linde, V. G. Weirs, Eds., Lecture Notes in Computational Science and Engineering, Vol. 41, Springer, 303–314.

Ducet, N., P. Y. Le Traon, and G. Reverdin, 2000: Global high-resolution mapping of ocean circulation from TOPEX/Poseidon and ERS-1 and -2. *J. Geophys. Res.,* **105** (C8), 19 477–19 498.

Eden, C., and C. Böning, 2002: Sources of eddy kinetic energy in the Labrador Sea. *J. Phys. Oceanogr.,* **32,** 3346–3363.

Emery, W. J., P. Brandt, A. Funk, and C. Böning, 2006: A comparison of sea surface temperatures from microwave remote sensing of the Labrador Sea with in situ measurements and model simulations. *J. Geophys. Res.,* **111,** C12013, doi:10.1029/2006JC003578.

Fischer, J., F. A. Schott, and M. Dengler, 2004: Boundary circulation at the exit of the Labrador Sea. *J. Phys. Oceanogr.,* **34,** 1548–1570.

Fox, A. D., and S. J. Maskell, 1995: Two-way interactive nesting of primitive equation ocean models with topography. *J. Phys. Oceanogr.,* **25,** 2977–2996.

——, and ——, 1996: A nested primitive equation model of the Iceland–Faeroe front. *J. Geophys. Res.,* **101,** 18 259–18 278.

Garnier, E., B. Barnier, L. Siefridt, and K. Béranger, 2000: Investigating the 15 years air–sea flux climatology from the ECMWF re-analysis project as a surface boundary condition for ocean models. *Int. J. Climatol.,* **20,** 1653–1673.

Gaspar, P., Y. Gregoris, and J. M. Lefevre, 1990: A simple eddy kinetic energy model for simulations of the oceanic vertical mixing: Tests at station Papa and long-term upper ocean study site. *J. Geophys. Res.,* **95,** 16 179–16 193.

Gent, P. R., and J. C. McWilliams, 1990: Isopycnal mixing in ocean circulation models. *J. Phys. Oceanogr.,* **20,** 150–155.

Jackett, D. R., and T. J. McDougall, 1995: Minimal adjustment of hydrographic data to achieve static stability. *J. Atmos. Oceanic Technol.,* **12,** 381–389.

Jones, H., and J. Marshall, 1993: Convection with rotation in a neutral ocean: A study of open-ocean deep convection. *J. Phys. Oceanogr.,* **23,** 1009–1039.

——, and ——, 1997: Restratification after deep convection. *J. Phys. Oceanogr.,* **27,** 2276–2286.

Käse, R. H., A. Biastoch, and D. B. Stammer, 2001: On the mid-depth circulation in the Labrador and Irminger Seas. *Geophys. Res. Lett.,* **28,** 3433–3436.

Katsman, C., M. Spall, and R. Pickart, 2004: Boundary current eddies and their role in the restratification of the Labrador Sea. *J. Phys. Oceanogr.,* **34,** 1967–1983.

Lavender, K., R. E. Davis, and W. B. Owens, 2000: Mid-depth recirculation observed in the interior Labrador and Irminger Seas by direct velocity measurements. *Nature,* **407,** 66–69.

Lazier, J., R. Hendry, A. Clarke, I. Yashayaev, and P. Rhines, 2002: Convection and restratification in the Labrador Sea, 1990–2000. *Deep-Sea Res. I,* **49,** 1819–1835.

Lilly, J. M., P. B. Rhines, M. Visbeck, R. Davis, J. Lazier, F. Schott, and D. Farmer, 1999: Observing deep convection in the Labrador Sea during winter 1994/95. *J. Phys. Oceanogr.,* **29,** 2065–2098.

——, ——, F. Schott, K. Lavender, J. Lazier, U. Send, and E. d'Asaro, 2003: Observations of the Labrador Sea eddy field. *Prog. Oceanogr.,* **59,** 75–176.

Madec, G., P. Delecluse, M. Imbard, and C. Levy, 1998: OPA 8.1 ocean general circulation model reference manual. IPSL Tech. Rep. 11, Institut Pierre-Simon Laplace, 91 pp.

Marshall, J., and F. Schott, 1999: Open-ocean convection: Observations, theory, and models. *Rev. Geophys.,* **37,** 1–64.

——, and Coauthors, 1998: The Labrador Sea Deep Convection Experiment. *Bull. Amer. Meteor. Soc.,* **79,** 2033–2058.

Mathiot, P., 2004: Turbulence mésoéchelle en mer du Labrador. Mémoire de maitrise de physique, Blaise Pascal University Press, 45 pp.

Mizoguchi, K., S. L. Morey, J. Zavala-Hidalgo, N. Suginohara, S. Häkkinen, and J. O'Brien, 2003: Convective activity in the Labrador Sea: Preconditioning associated with decadal variability in subsurface ocean stratification. *J. Geophys. Res.,* **108,** 3330, doi:10.1029/2002JC001735.

Penven, P., L. Debreu, P. Marchesiello, and J. C. McWilliams, 2006: Evaluation and application of the ROMS 1-way embedding procedure to the central California upwelling system. *Ocean Modell.,* **12,** 157–187.

Pickart, R. S., D. J. Torres, and R. A. Clarke, 2002: Hydrography of the Labrador Sea during active convection. *J. Phys. Oceanogr.,* **32,** 428–457.

Prater, M. D., 2002: Eddies in the Labrador Sea as observed by profiling RAFOS floats and remote sensing. *J. Phys. Oceanogr.,* **32,** 411–427.

Reynaud, T. H., P. Legrand, H. Mercier, and B. Barnier, 1998: A new analysis of hydrographic data in the Atlantic and its application to an inverse modelling study. *International WOCE Newsletter,* No. 32, WOCE International Project Office, Southampton, United Kingdom, 29–31.

Reynolds, R. W., and T. M. Smith, 1994: Improved global sea surface temperature analyses using optimum interpolation. *J. Climate,* **7,** 929–948.

Smith, W., and D. Sandwell, 1997: Global sea floor topography from satellite altimetry and ship depth soundings. *Science,* **277,** 1957–1962.

Spall, M. A., 2004: Boundary currents and water mass transformation in marginal seas. *J. Phys. Oceanogr.,* **34,** 1197–1213.

——, and W. R. Holland, 1991: A nested primitive equation model for oceanic applications. *J. Phys. Oceanogr.,* **21,** 205–220.

Straneo, F., 2006: Heat and freshwater transport through the central Labrador Sea. *J. Phys. Oceanogr.,* **36,** 606–628.

——, R. Pickart, and K. Lavender, 2003: Spreading of Labrador Sea Water: An advective–diffusive study based on Lagrangian data. *Deep-Sea Res. I,* **50,** 701–719.

Treguier, A. M., S. Theetten, E. P. Chassignet, T. Penduff, R. Smith, L. Talley, J. O. Beismann, and C. Böning, 2005: The North Atlantic subpolar gyre in four high-resolution models. *J. Phys. Oceanogr.,* **35,** 757–774.

Visbeck, M., J. Marshall, and H. Jones, 1996: Dynamics of isolated convective regions in the ocean. *J. Phys. Oceanogr.,* **26,** 1721–1734.

Willebrand, J., and Coauthors, 2001: Circulation characteristics in three eddy-permitting models of the North Atlantic. *Prog. Oceanogr.,* **48,** 123–161.